Originally published as:

Ojha, N., Naja, M., Singh, K. P., Sarangi, T., Kumar, R., Lal, S., Lawrence, M. G., Butler, T. M., Chandola, H. C. (2012): Variabilities in ozone at a semi-urban site in the Indo-Gangetic Plain region: Association with the meteorology and regional processes. - *Journal of Geophysical Research: Atmospheres*, *117*, 20, D20301.

DOI: http://doi.org/10.1029/2012JD017716

Variabilities in ozone at a semi-urban site in the Indo-Gangetic Plain region: Association with the meteorology and regional processes

Narendra Ojha,[1,2] Manish Naja,[1,2] K. P. Singh,[3] T. Sarangi,[1,2] R. Kumar,[1] S. Lal,[4] M. G. Lawrence,[5,6] T. M. Butler,[5,6] and H. C. Chandola[2]

Received 1 March 2012; revised 12 September 2012; accepted 12 September 2012; published 19 October 2012.

[1] The Indo-Gangetic Plain (IGP) region is one of the most densely populated regions in the World, but ground-based observations of air pollutants are highly limited in this region. Here, surface ozone observations made during March 2009–June 2011 at a semi-urban site (Pantnagar; 29.0°N, 79.5°E, 231 m amsl) in the IGP region are presented. Ozone mixing ratios show a daytime photochemical buildup with ozone levels sometimes as high as 100 ppbv. Seasonal variation in 24-h average ozone shows a distinct spring maximum (39.3 ± 18.9 ppbv in May) while daytime (1130–1630 h) average ozone shows an additional peak during autumn (48.7 ± 13.8 ppbv in November). The daytime, but not daily average, observed ozone seasonality is in agreement with the space-borne observations of OMI tropospheric column NO_2, TES CO (681 hPa), surface ozone observations at a nearby high altitude site (Nainital) in the central Himalayas and to an extent with results from a global chemistry transport model (MATCH-MPIC). It is suggested that spring and autumn ozone maximum are mainly due to photochemistry, involving local pollutants and small-scale dynamical processes. Biomass burning activity over the northern Indian region could act as an additional source of ozone precursors during spring. The seasonal ozone photochemical buildup is estimated to be 32–41 ppbv during spring and autumn and 9–14 ppbv during August–September. A correlation analysis between ozone levels at Pantnagar and Nainital along with the mixing depth data suggests that emissions and photochemical processes in the IGP region influence the air quality of pristine Himalayan region, particularly during midday hours of spring. The evening rate of change (8.5 ppbv hr^{-1}) is higher than the morning rate of change, which is dissimilar to those at other urban or rural sites. Ozone seasonality over the IGP region is different than that over southern India. Results from the MATCH-MPIC model capture observed ozone seasonality but overestimate ozone levels. Model simulated daytime ratios of H_2O_2/HNO_3 are higher and suggesting that this region is in a NO_x-limited regime. A chemical box model (NACR Master Mechanism) is used to further corroborate this using a set of sensitivity simulations, and to estimate the integrated net ozone production in a day (72.9 ppbv) at this site.

Citation: Ojha, N., M. Naja, K. P. Singh, T. Sarangi, R. Kumar, S. Lal, M. G. Lawrence, T. M. Butler, and H. C. Chandola (2012), Variabilities in ozone at a semi-urban site in the Indo-Gangetic Plain region: Association with the meteorology and regional processes, *J. Geophys. Res.*, *117*, D20301, doi:10.1029/2012JD017716.

[1]Aryabhatta Research Institute of Observational Sciences, Nainital, India.
[2]Department of Physics, Kumaun University, Nainital, India.
[3]Biophysics and Nanobiosensor Research Laboratory, College of Basic Sciences and Humanities, G. B. Pant University of Agriculture and Technology, Pantnagar, India.
[4]Physical Research Laboratory, Ahmedabad, India.
[5]Max Planck Institute for Chemistry, Mainz, Germany.
[6]Institute for Advanced Sustainability Studies, Potsdam, Germany.

Corresponding author: M. Naja, Aryabhatta Research Institute of Observational Sciences, Manora Peak, Nainital Uttarakhand 263129, India. (manish@aries.res.in)

1. Introduction

[2] Tropospheric ozone is an important secondary pollutant due to its adverse effects on living beings [*Desqueyroux et al.*, 2002] and vegetation [*Mauzerall and Wang*, 2001]. It also plays a vital role in atmospheric chemistry as a major precursor of the OH radical, which removes a large number of organic compounds and some other pollutants from the atmosphere and controls its oxidizing capacity [*Thompson*, 1992; *Cantrell and Orlando*, 1999]. Additionally, higher radiative forcing of tropospheric ozone (1200–2000 times higher than that of CO_2 molecule) on a per molecule basis [*Schwarzkopf and Ramaswamy*, 1993] makes it a potent

global warming agent. It has been ranked the third most important greenhouse gas with a global mean radiative forcing of 0.35 ± 0.15 W m^{-2} [*Forster et al.*, 2007].

[3] Detailed observations of ozone and other trace species over South Asia are relatively scarce, where human population and the anthropogenic emissions of several key trace species have been increasing rapidly for the past few decades [e.g., *Akimoto*, 2003; *Ohara et al.*, 2007]. South Asia is also home to five megacities (Delhi, Dhaka, Mumbai, Karachi, and Kolkata) and the Indo-Gangetic Plain (IGP) region, which is one of the most populated regions of the world. Tropospheric ozone studies over this region have additional importance due to higher photochemical activities associated with strong tropical insolation and higher water vapor content. Further, strong convection in the tropical regions may lift the pollutants to higher altitudes from where they can be transported to other parts of the world. For example, convection associated with monsoonal circulation can transport South Asian pollutants to the Mediterranean Sea [e.g., *Lawrence et al.*, 2003; *Park et al.*, 2007]. Further, the chemical characteristics of South Asian emissions are different from those in other parts of the world because of their disproportionately large contribution from bio-fuel and biomass burning [e.g., *Lawrence and Lelieveld*, 2010].

[4] Previous observations of surface ozone over the Indian region were confined mostly to the western and southern regions [e.g., *Lal et al.*, 2000; *Naja and Lal*, 2002; *Beig et al.*, 2007; *Reddy et al.*, 2008]. However, observations are sparse in the Northern India, where only two sites have observations of a complete ozone seasonal cycle. One site is a highly urbanized megacity (Delhi) [*Ghude et al.*, 2008] and other one is a high altitude cleaner site in the central Himalayan region (Nainital) [*Kumar et al.*, 2010].

[5] The Indo-Gangetic Plain (IGP) region in Northern India encompasses a variety of anthropogenic and biogenic emission sources. This region stretches from the Indus river system in Pakistan to the delta of Ganges River in Bangladesh in the west-east direction. The high altitude Himalayan range is the northern border and the plateau of Deccan is on the south side. There are diverse emission sources, such as coal based thermal power plants, different industries, mobile sources, bio-fuel burning, mining, and crop residue burning in the IGP region. Analysis of emission fluxes from INTEX-B inventory [*Zhang et al.*, 2009] shows that CO, NO_x and NMVOC emissions over the IGP region (CO: 200 to 700 mol km^{-2} hr^{-1}, NO_x: 5 to 20 mol km^{-2} hr^{-1} and NMVOC: 30 to 50 mol km^{-2} hr^{-1}) are significantly higher than those over the rest of the India (CO: 50 to 200 mol km^{-2} hr^{-1}, NO_x: 3 to 10 mol km^{-2} hr^{-1}, NMVOC: $\sim$5 to 30 mol km^{-2} hr^{-1}). Pollutants emitted from the IGP region, get trapped by the complex hilly terrain in the north and northeast, which induces elevated levels of pollutants, both gases as well as aerosols. This has been reported using satellite based observations of total tropospheric ozone, CO, NO_2 and aerosol properties [*Fishman et al.*, 2003; *Di Girolamo et al.*, 2004; *Jethva et al.*, 2005; *Gautam et al.*, 2009; *Kar et al.*, 2010; *Giles et al.*, 2011]. The outflow of pollutants from the IGP region further influences the pristine oceanic region adjoining India [*Lelieveld et al.*, 2001; *Lal et al.*, 2007; *Srivastava et al.*, 2011]. Despite these, observations of trace gases are nearly non-existing in the IGP region.

[6] In light of the above conditions, surface ozone measurements were initiated at a semi-urban site Pantnagar in the IGP region. Variations in surface ozone at Pantnagar are analyzed using different meteorological parameters (solar radiation, temperature, rainfall and mixing depth), backward trajectory and space-borne observations. Ozone seasonality at Pantnagar is also compared with the available observations over other sites in India, particularly with a nearby high altitude site in the central Himalayas, and with the result of a global chemistry transport model (MATCH-MPIC). A chemical box-model (NCAR-MM) is employed to calculate ozone production $P(O_3)$ and to study dependence of ozone mixing ratios on Non-Methane Hydrocarbons (NMHCs) and NO_x.

2. Observation Site, Techniques and Data Analysis

[7] Surface ozone measurements are made at the College of Basic Sciences and Humanities (CBSH), G. B. Pant University of Agriculture and Technology (GBPUAT), Pantnagar (29.0°N, 79.5°E, 231 m amsl) during March 2009–June 2011. Figure 1 shows the geographical location of the observation site overlaid on the topography and population density (CIESIN; http://sedac.ciesin.columbia.edu/gpw) map of the Northern Indian region. The high altitude Himalayan Mountains lie in the Northern and Eastern sectors of the observation site, while low altitude plains are located in the South and West of the site (Figure 1a). Mountains of 1500–2000 m altitude are about 50 km away and mountains of 4000–5000 m altitude range are about 130 km away from the observation site. The population density is 250–1000 persons per km^2 around Pantnagar and it is much less (25–250 persons per km^2) in the Northern region (Figure 1b). The university campus has a perimeter of about 30 km and encompasses a large area of about 16000 acres (about 65 km^2) and is used primarily for the agricultural research. There is no major source of emissions in the observation site vicinity, except the local vehicular movement inside the university campus. Some small-scale industries are located in the nearby towns: Rudrapur (12 km southwest of Pantnagar) and Haldwani (25 km northeast of Pantnagar). Delhi is the nearest megacity, located about 225 km southwest of Pantnagar (Figure 1). Annual average anthropogenic emissions (INTEX-B) [*Zhang et al.*, 2009] of CO over Indian region (Figure 1c) clearly indicate that emissions are significantly higher over the Northern India. The spread of higher CO emissions from North to East is largely representing the Indo-Gangetic plain (IGP) region (Figure 1c). As mentioned earlier, anthropogenic emissions of ozone precursors are significantly higher over the IGP region as compared to average emissions over the rest of the India.

2.1. Measurements of Ozone, CO and CH_4

[8] Surface ozone measurements made using online ozone analyzers (Teledyne M400E and Thermo Model-49i) are based on the well-known technique of UV light absorption by ozone molecules at 254 nm. These analyzers have a response time of about 20 s and a minimum detection limit of about one ppbv. The ambient air inside the analyzer is drawn through a Teflon tube from the rooftop of the second

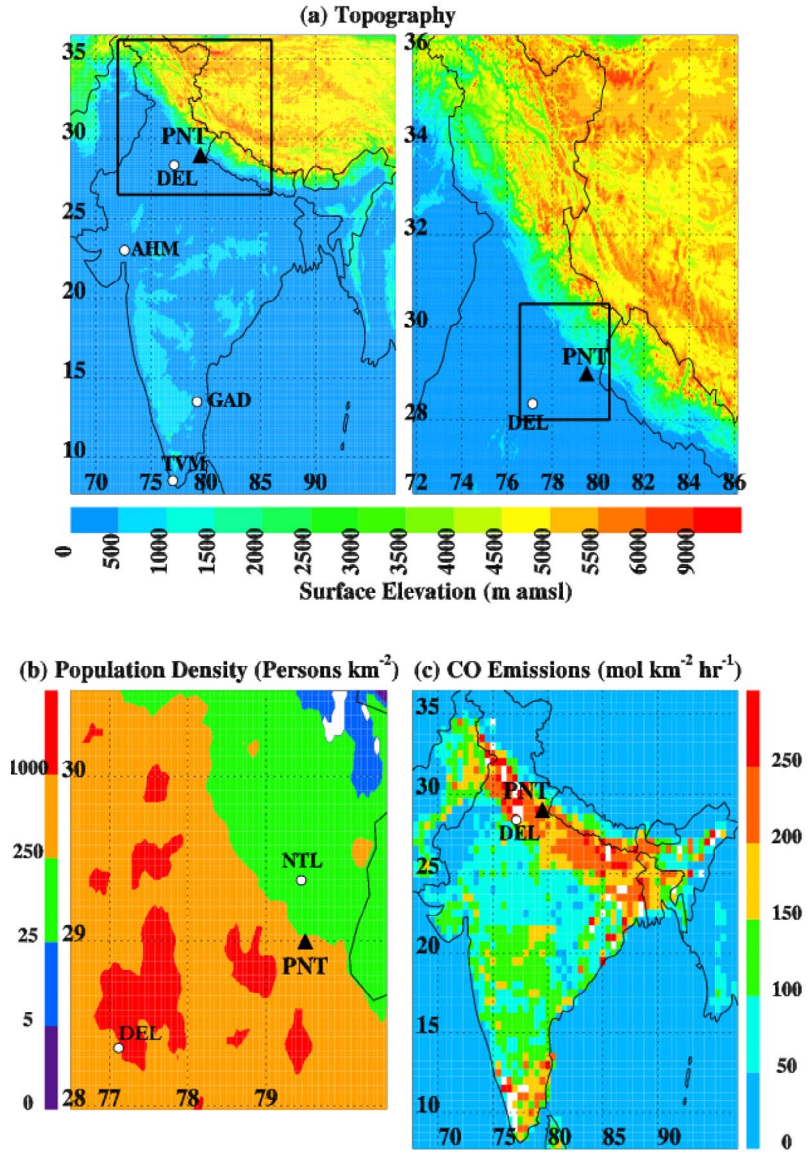

Figure 1. (a) Topographical map of India with zoomed map of the northern India, (b) population density around the observation site, and (c) annual average CO emissions (INTEX-B) over India are shown. A belt of higher CO emissions, from the northern India to the eastern side, is the IGP region. Observation site Pantnagar (PNT) is marked with a black filled triangle, other sites used for comparison namely Delhi (DEL), Ahmedabad (AHM), Gadanki (GAD), Trivandrum (TVM) and Nainital (NTL) are marked with white filled circles.

floor with a flow of about 1 L per min. The absolute accuracy of this system is about 5% [*Kleinman et al.*, 1994]. Average ozone values are stored over 15 min intervals and used for further analysis. The accuracy of both the analyzers is examined periodically by performing zero and span checks. Ozone observations from both the analyzers have been inter-compared by running them side by side using a common inlet system and both the analyzers showed very strong positive correlation (r^2 = 0.95). Further details of ozone observations by such instruments can be seen elsewhere [e.g., *Naja and Lal*, 2002; *Kumar et al.*, 2010, 2011]. Air samples have also been collected from Pantnagar and from a nearby site Haldwani in pre-evacuated glass bottles using a metal bellow pump at a pressure of 1.6 bar for the analysis of CO and CH_4. The total number of samples collected for each month is mentioned in Table 1. Very few samples were analyzed for light NMHCs (C_2–C_5). These data are not discussed here but they are used in initializing box model simulation (section 3.5). Similarly, NO_x observations were made for few days, using a chemiluminescence analyzer (Teledyne model – 200 EU) and used here only for the box-model setup. Air samples analyzed using a Gas Chromatograph (GC) coupled with a Flame Ionization Detector (FID) with a heated Ni catalyst at Physical Research Laboratory, Ahmedabad. Calibration mixtures from NIST (USA) and Matheson (USA) were used for the calibration of CH_4

Table 1. Monthly Average Mixing Depth, Monthly Average Ozone With One Sigma Deviation, Maximum Ozone, Number of Ozone Data Counts (15 min Average), Average CO, Average CH_4 and Number of Samples During Study Period at Pantnagar

Month	Mixing Depth (m AGL)	Ozone (ppbv)	Maximum	Ozone Count	CO (ppbv)	CH_4 (ppmv)	Sample Count
Jan	597 ± 335	10.8 ± 12.1	50	2918	400.7 ± 274.2	2.11 ± 0.22	5
Feb	855 ± 429	18.1 ± 14.7	67	4020	-	-	-
Mar	1476 ± 664	27.0 ± 18.8	97	6376	484.4 ± 114.8	1.94 ± 0.17	5
Apr	2621 ± 749	34.5 ± 20.3	95	4009	292.3 ± 188.6	1.82 ± 0.03	12
May	2556 ± 722	39.3 ± 18.9	105	5777	399.2 ± 204.4	1.82 ± 0.03	12
Jun	2399 ± 849	34.8 ± 18.4	103	6343	187.6 ± 14.9	1.81 ± 0.03	2
Jul	1256 ± 573	19.6 ± 12.7	69	2819	277.1 ± 100.3	1.85 ± 0.05	8
Aug	884 ± 290	16.8 ± 8.9	81	1693	291.2 ± 124.9	1.86 ± 0.11	6
Sep	627 ± 271	17.4 ± 10.8	56	3581	425.4 ± 148.9	2.11 ± 0.18	3
Oct	614 ± 361	19.7 ± 17.7	78	4760	339.8 ± 106.6	2.11 ± 0.08	4
Nov	616 ± 317	20.0 ± 19.1	83	4449	409.9 ± 199.7	2.09 ± 0.19	5
Dec	610 ± 299	16.1 ± 17.2	62	2453	205.1	1.81	1
Annual	1358 ± 982	25.0 ± 19.2	105	49198[a]	348.5 ± 176.7	1.91 ± 0.16	63[a]

[a]Total.

and CO and the reproducibility of the analysis is better than 1% and 6% respectively. Further details regarding the calibration and accuracy of this set up is available in *Lal et al.* [2007].

2.2. Satellite Data

[9] This study uses monthly rainfall data (2009–2010) from the Tropical Rainfall Measuring Mission (TRMM 3B43 V6) at 0.25° × 0.25° spatial resolution to examine seasonal variations in rainfall. Ozone Monitoring Instrument (OMI) retrieved tropospheric column NO_2 (OMNO2e.003) version-3 and Level-3 daily data at 0.25° × 0.25° resolution are used to study variations in NO_2. Additionally, Level 3 tropospheric column ozone and CO at 681 hPa data from the Tropospheric Emission spectrometer (TES) are also used.

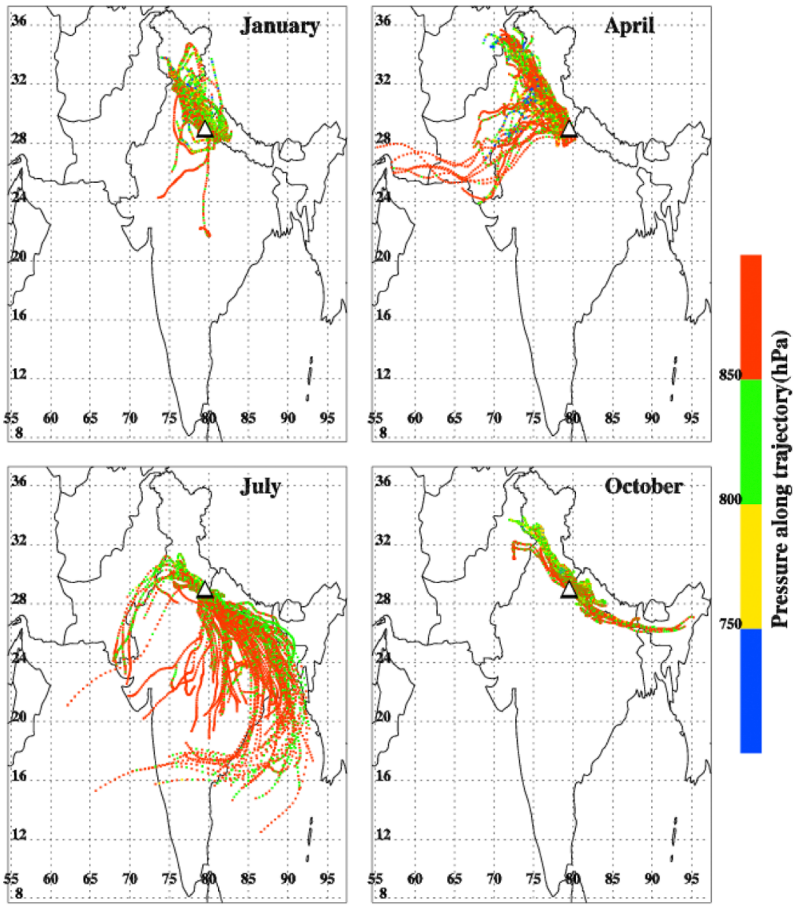

Figure 2. Three days backward (1000 m AGL) trajectories at Pantnagar for all days in January, April, July and October 2010 are shown. The trajectories are color coded, according to the atmospheric pressure along the trajectories, to portray the altitude range attained by the air masses before arriving at the observation site.

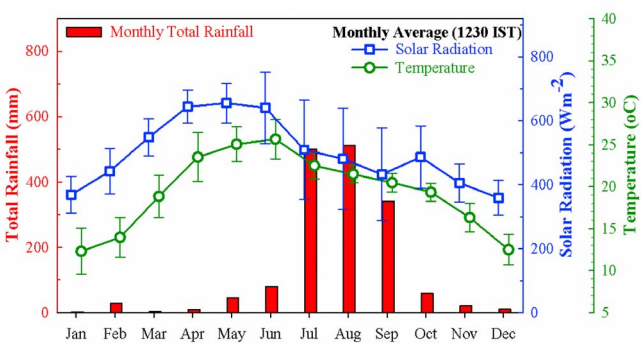

Figure 3. Seasonal variations in monthly total rainfall from TRMM (2009–2010), solar radiation (Wm^{-2}) and temperature from GDAS data (2009–2011) over Pantnagar.

TES CO retrievals are used at 681 hPa because TES has higher sensitivity at this level [*Rinsland et al.*, 2006]. More details regarding the measurements by TRMM, OMI and TES can be seen in the work of *Adler et al.* [2000], *Beer et al.* [2001], and *Bucsela et al.* [2006], respectively.

2.3. General Meteorology

[10] Three day backward trajectories are simulated at Pantnagar at an altitude of 1000 m above ground level (AGL) during January, April, July and October representing winter, spring, summer-monsoon and autumn (Figure 2) using the HYSPLIT (Hybrid Single Particle Lagrangian Integrated Trajectory) model (http://www.arl.noaa.gov/HYSPLIT_info.php). The trajectories are color coded according to atmospheric pressure along the trajectory to portray the altitude range attained by the air masses before arriving at the observation site. Wind patterns over this region are northerly or northwesterly during winter. Air masses mostly circulate over the continental Indian region including polluted IGP region during spring and autumn before reaching at the observation site. While cleaner marine air masses arrive at this region during the summer-monsoon. Such seasonal changes in the synoptic wind pattern are generally observed every year over this region [*Asnani*, 2005]. Data analysis of these three day backward trajectories shows that air masses are mostly within the boundary layer, particularly during spring when the average mixing depth is higher (about 2500 m, Table 1).

[11] In situ measurements of meteorological parameters are not available at the site during the study period, therefore, GDAS data (ftp://gdas-server.iarc.uaf.edu/gdas1/), available every 6 h at the spatial resolution of 1° × 1° have been used to obtain solar radiation, temperature and mixing depth using HYSPLIT model (R. R. Draxler and G. D. Rolph, HYSPLIT (HYbrid Single-Particle Lagrangian Integrated Trajectory) Model, 2012, http://ready.arl.noaa.gov/HYSPLIT.php). HYSPLIT simulated solar radiation data has been compared with NCEP reanalysis solar radiation data during 2009–2010 period that shows a good agreement ($r^2 = 0.98$) (auxiliary material Figure S1).[1] The mixing depth is estimated using Turbulent Kinetic Energy (TKE) profile method, in which mixing depth is assigned to the height at which TKE either decreases by a factor of two or to a value less than 0.21. Further details regarding mixing depth estimation using HYSPLIT model are available elsewhere [*Draxler et al.*, 2012]. To study diurnal variations in the mixing depth in different months, model calculations are also made every hour from 10th day to 20th day of that month and monthly average diurnal variations have been calculated.

[12] Figure 3 shows the seasonal variations in the solar radiation, temperature and rainfall over Pantnagar. Solar radiation (noontime 1230 h) is lower during winter as generally foggy conditions prevail over this region during this period. Solar radiation shows a systematic increase from January to June and is most intense during spring months (Apr to June). Arrival of monsoon causes cloudy and rainy conditions leading to drastic reduction in solar radiation during July, August and September coinciding with the maximum rainfall. Solar radiation shows a recovery then after resulting in a secondary maximum during autumn. Temperature also shows more or less similar variations to solar radiation and shows a springtime maximum (∼26°C) and wintertime minimum (∼12°C).

2.4. Global Chemistry Transport Model: MATCH-MPIC

[13] Spatial and temporal variations in ozone and related species are also obtained from the offline global chemistry transport model MATCH-MPIC (Model of Atmospheric Transport and CHemistry – Max Planck Institute for Chemistry version 3.0). MATCH-MPIC was developed at the National Center for Atmospheric Research and the Max Planck Institute for Chemistry (http://cwf.mpic.de/∼cwf/match/match_overview.html). The version from *Lawrence et al.* [2003] developed for chemical weather forecasts is used here, with a few updates, most importantly at a higher resolution (T106 versus T42), and with updated emissions. The simulations here are driven by NCEP/NCAR reanalysis meteorology data at T106 horizontal resolution (∼0.9° × 0.9°) with 42 vertical levels (from the surface to ∼2 hPa) available every 3 h. A time step of 10 min is used in the simulations. The meteorology component of MATCH uses the NCEP data to simulate advective transport [*Rasch and Lawrence*, 1998], and also to diagnose convection [*Zhang and McFarlane*, 1995; *Hack et al.*, 1994], vertical diffusion [*Holtslag and Boville*, 1993], cloud fractions [*Slingo*, 1987], and cloud microphysics [*Rasch and Kristjánsson*, 1998]. Unlike most offline models, MATCH has a full tropospheric hydrological cycle; the surface source of water vapor is computed from the latent heat flux in the NCEP data, and the moisture transport and precipitation are computed using the algorithms in MATCH. This gives a water vapor distribution, which is internally consistent with the model's meteorology [*Rasch et al.*, 1997; *Lawrence et al.*, 1999].

[14] The tropospheric chemistry module includes isoprene chemistry based on the Mainz Isoprene Mechanism [*Pöschl et al.*, 2000], as well as representations of ethane, propane, ethene, propene, and n-butane [*von Kuhlmann et al.*, 2003]. Surface emissions of CO, NO_x, and non-methane hydrocarbons for industrial sources are taken from EDGAR inventory [*Olivier et al.*, 1999]. Biomass burning emissions

[1] Auxiliary materials are available in the HTML. doi:10.1029/2012JD017716.

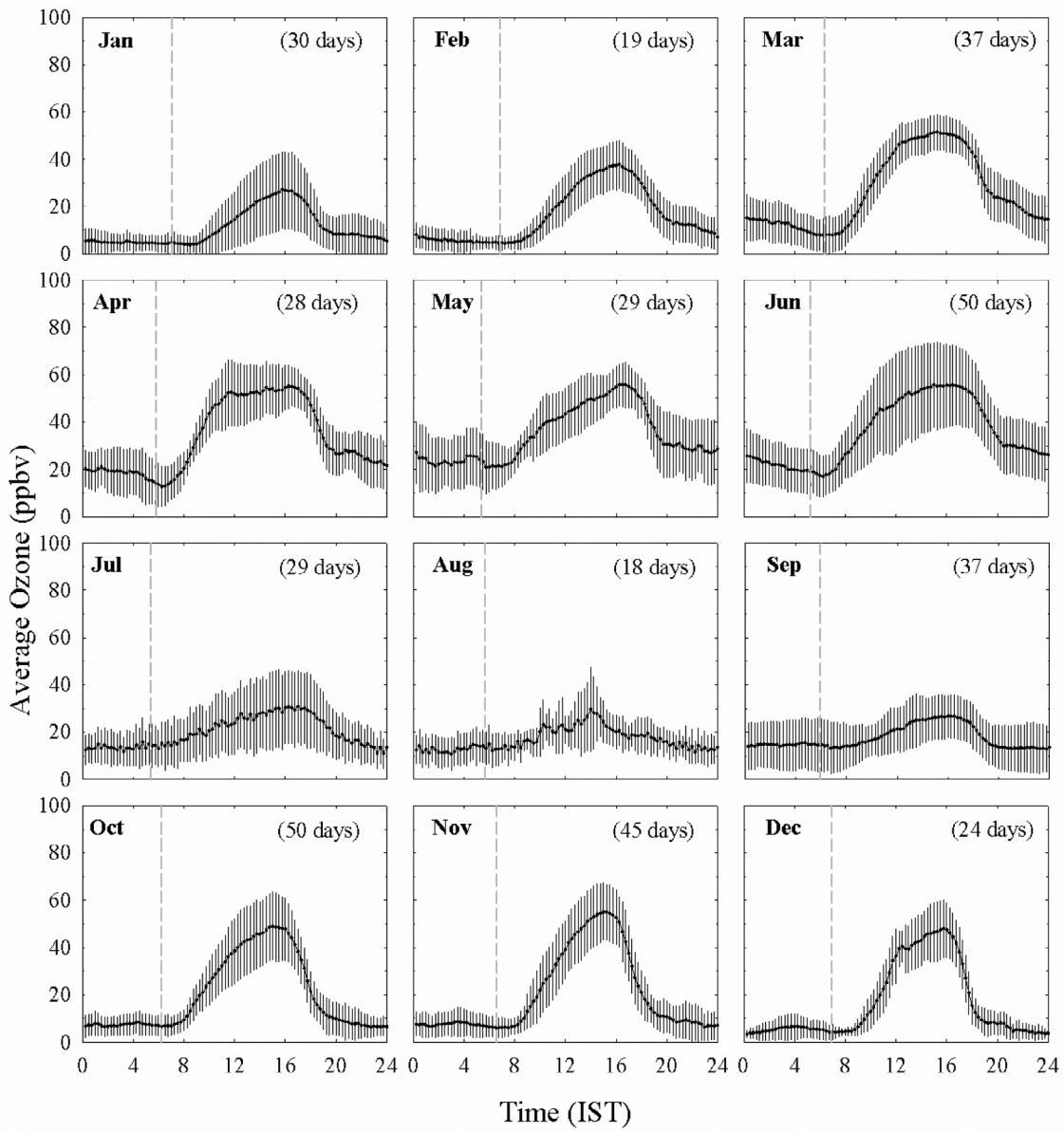

Figure 4. Monthly average diurnal variation in ozone at Pantnagar from January to December during March 2009 to June 2011 period. Sunrise times in these months are also shown as dotted lines and total numbers of days for which observations are available in each month are mentioned in the upper right corner in each month plot.

are based on climatological emissions from GFEDv2 [*van der Werf et al.*, 2006]. Soil NO_x emissions are taken from *Yienger and Levy* [1995]. Lightning NO_x emissions are calculated online based on convective mass flux, with the global lightning NO_x emissions scaled to 2 Tg(N)/yr. Aircraft emissions are taken from *Schmitt and Brunner* [1997]. Photolysis rates are computed using online actinic flux calculations at eight representative wavelengths, and the modeled cloud fractions and ozone profiles. Based on the technique of *Landgraf and Crutzen* [1998], including consideration of modeled cloud and O_3 profiles. Dry deposition is from *Ganzeveld and Lelieveld* [1995], and heterogeneous loss of N_2O_5 on aerosols is based on *Dentener and Crutzen* [1993]. Cloud scavenging by precipitation and gravitational settling processes in non-precipitating clouds are computed based on the modeled precipitation production rates in each grid cell, as described in *Lawrence and Crutzen* [1998] and *Crutzen and Lawrence* [2000].

[15] Over the Asian region, this model is shown to reproduce the NO_x variability well including the enhanced abundances of NO_2 over China and northeast India, in addition to the higher levels during the biomass burning periods, however, the absolute levels were somewhat underestimated [*Kunhikrishnan et al.*, 2004]. Further details of MATCH-MPIC description as well as evaluation can be found elsewhere [*Rasch et al.*, 1997; *Lawrence et al.*, 1999;

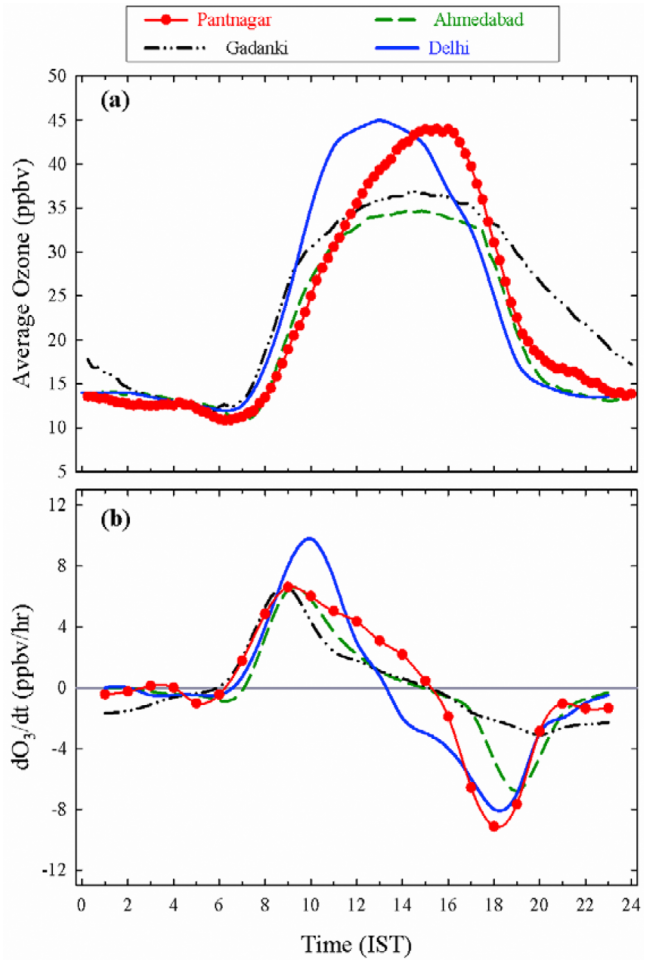

Figure 5. (a) Average diurnal variations in ozone and (b) diurnal variation in rate of change of ozone (ppbv/hour) at Pantnagar along with those at Delhi [*Ghude et al.*, 2008], Ahmedabad [*Lal et al.*, 2000] and Gadanki [*Naja and Lal*, 2002].

von Kuhlmann, 2001; *von Kuhlmann et al.*, 2003; *Lawrence et al.*, 2003].

2.5. Chemical Box Model

[16] A chemical box model (NCAR-MM) developed at National Center for Atmospheric Research, Boulder, USA, is employed for simulating the diurnal variations in surface ozone and for investigating the sensitivity of ozone variations to changes in NO_x and NMHCs. This model consists of highly detailed gas phase chemistry with about 2000 species participating in about 5000 reactions and can simulate the time evolution of an air parcel initialized with known concentrations assuming no further dilution, emissions, and transport (http://cprm.acd.ucar.edu/Models/MasterMech/index.shtml). In this study, the model is initialized with O_3, H_2O, NO, NO_2, CO, OH, HO_2, CH_2O, CH_4, i-butane, n-butane, Isoprene, Xylene, and Toluene while N_2, O_2, M and photons are hard-wired. Photolysis rate coefficients i.e., j-values are estimated using the Tropospheric Ultraviolet Visible (TUV) radiative transfer model [*Madronich and Flocke*, 1999] with 4-stream discrete ordinates radiative transfer solver [*Stamnes et al.*, 1998]. Further details of the NCAR-MM model can be seen elsewhere [*Madronich*, 2006].

3. Results

3.1. Diurnal Variations in Ozone

[17] Monthly average ozone diurnal variations from January to December during March 2009–June 2011 period at Pantnagar are shown in Figure 4. These diurnal variations are characterized by higher values during daytime and lower values during nighttime. Daytime build up is observed throughout the year, except some cloudy/rainy days during July to September. Such diurnal variations are common at urban and rural sites and are attributed mainly to the daytime in situ photochemical production of ozone from its precursors including NO_x, CO, and VOCs [e.g., *Kleinman et al.*, 1994; *Naja and Lal*, 2002]. However, the dependence of ozone production on the concentrations of its precursors is complex and nonlinear [e.g., *Lin et al.*, 1988], and will be discussed later in detail using a chemical box model (see section 3.5). Lower ozone levels during the nighttime are largely associated with the titration of ozone by NO and deposition of ozone. During March to June, ozone mixing ratios attain the lowest value during early morning (just after sunrise). This could be due to ozone losses through reactions with NO and NO_2, which maybe produced by photo dissociation of NO_3 and N_2O_5 accumulated overnight. Such minimum in the ozone levels just after sunrise has also been reported from another urban site in India [*Lal et al.*, 2000]. In addition to photochemistry, the evolution of the boundary layer during daytime, has also been suggested to contribute to the ozone variations through mixing of near surface air having lower ozone levels with the ozone rich air aloft [*Zhang and Rao*, 1999; *Rao et al.*, 2003].

3.1.1. Rate of Change in Ozone

[18] The morning and evening time rates of change of ozone can be used as an indicator of the chemical environment (i.e., urban or rural) prevailing over a site [e.g., *Naja and Lal*, 2002]. Urban sites generally show symmetric diurnal patterns, i.e., rates of change in ozone during morning and evening hours are similar, while rural sites are characterized by lower loss rates during evening hours. Morning time rate of increase of ozone i.e., ozone formation process strongly depends upon the available amount of precursors, while evening time loss rate i.e., ozone titration process would mainly depend upon the NO levels.

[19] Generally, over the Indian region, NO levels are observed to be lower at rural sites in comparison with those at urban sites, which lead to slower ozone titration by NO during evening hours at a rural site [e.g., *Naja and Lal*, 2002]. In view of this, diurnal variations in average ozone mixing ratios at Pantnagar are compared with those observed at other urban (Delhi and Ahmedabad) and rural (Gadanki) sites in India (Figure 5a). The diurnal variations in the rates of change in ozone (ppbv/hour) are also calculated at these four sites (Figure 5b). The ozone decrease during evening time at Pantnagar is comparable to those at Ahmedabad and Delhi, while the decrease in ozone is slower at Gadanki (Figure 5b).

[20] Morning (0800–1100 h) and evening (1700–1900 h) time rates of change in ozone are compared among these four sites for annual data set (Table 2). For Pantnagar site,

Table 2. Comparison of Rate of Change of Ozone at Pantnagar With Those at Other Sites in India[a]

Sites	Rate of Change During 0800–1100 h IST (ppbv/hr)	Rate of Change During 1700–1900 h IST (ppbv/hr)	Reference
Delhi	+8.3	−7.5	*Ghude et al.* [2008]
Ahmedabad	+5.9	−6.4	*Lal et al.* [2000]
Gadanki	+4.6	−2.6	*Naja and Lal* [2002]
Pantnagar	All data: +5.6 ± 2.9	All data: −8.5 ± 4.4	Present study
	Winter(DJF): +4.6 ± 2.0	Winter(DJF): −10.3 ± 4.0	Present study
	Spring(MAM): +8.4 ± 2.4	Spring(MAM): −10.6 ± 0.5	Present study
	Summer(JJA): +3.6 ± 2.1	Summer(JJA): −3.0 ± 2.8	Present study
	Autumn(SON): +5.6 ± 3.5	Autumn(SON): −10.0 ± 4.6	Present study

[a]Positive rate is for increase in ozone while negative is indication for decrease in ozone.

the morning and evening time rate of change of ozone are also estimated for different seasons. Urban sites (Delhi and Ahmedabad) show nearly similar magnitude of morning and evening rates of change whereas the evening rate of change at the rural site (Gadanki) is lower than that during morning hours. In contrast, morning and evening rates are not similar at Pantnagar; in addition, the evening rate of change (8.5 ppbv hr^{-1}) is higher than morning rate of change (5.6 ppbv hr^{-1}). This suggests that the ozone loss process via NO titration could be stronger at Pantnagar than that at Gadanki indicating that NO_x emissions could be higher over this region (IGP) when compared with those over the Southern region (e.g., Gadanki). The difference in ozone rate of change between daytime and nighttime is much greater during winter and autumn when compared with spring and summer at Pantnagar (Table 2).

3.2. Seasonal Variation in Ozone

[21] The seasonal variation in monthly average ozone mixing ratios at Pantnagar is depicted in Figure 6 along with variations in daily (24-h) average and daytime (1130–1630 h) hourly average ozone. The daily and monthly average ozone mixing ratios at Pantnagar show a systematic increase from January to May, decrease sharply in mid June to attain very low levels (10–30 ppbv) that endure until September, and a slight increase during October–November. The seasonal variations in daytime and nighttime average ozone levels (Figure 6) are similar to all data monthly average except during October–December, when daytime levels show a sharp increase and thus a secondary maximum that is not seen in all data monthly average. Nighttime data show lower values during October–December. The monthly statistics of surface ozone mixing ratios at Pantnagar is shown in Table 1. Average ozone levels are observed to be highest (39.3 ± 18.9 ppbv) in May, while these are lower in January (10.8 ± 12.1 ppbv) and summer-monsoon (16.8 ± 8.9 in August). Although monthly average ozone levels remain below 40 ppbv throughout the year but hourly average ozone levels in excess of 80 ppbv are observed occasionally particularly during spring (Figure 6). Average CO values, derived from whole air samples at Pantnagar, are moderately high (188–484 ppbv) while average CH_4 values range from 1.81 to 2.11 ppmv.

[22] Since in situ observations of CO and NO_2 are not available with sufficient temporal resolution at Pantnagar, data from space-borne sensors are used to examine seasonal variations in CO and NO_2. TES CO (at 681 hPa), OMI tropospheric column NO_2 and TES tropospheric column ozone are obtained over a 1° × 1° grid box centered at Pantnagar. The seasonal variations in OMI tropospheric column NO_2,

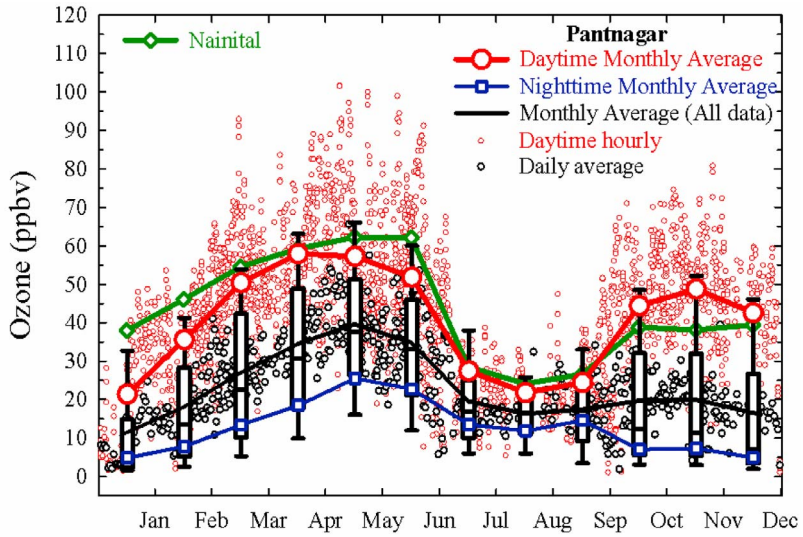

Figure 6. Seasonal variations in monthly (24 h), daily (24 h), daytime (1130–1630 h) and nighttime (0100–0300 h) average ozone at Pantnagar. Monthly average ozone mixing ratios at a nearby high altitude site (Nainital) are also shown.

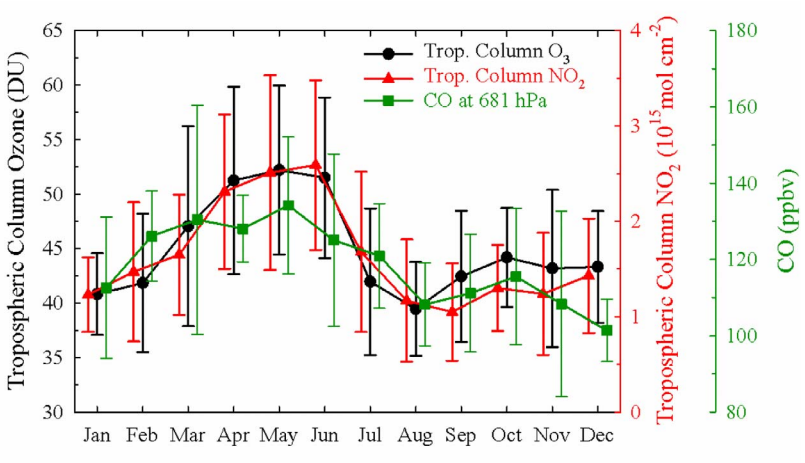

Figure 7. Seasonal variations in the tropospheric column ozone, tropospheric column NO_2 and CO at 681 hPa over Pantnagar.

TES CO and TES tropospheric column ozone are similar with highest values during spring and lower during summer/monsoon (Figure 7). A secondary maximum in these space-borne observations of ozone, NO_2 and CO during autumn is also seen similar to the daytime average surface ozone observed at Pantnagar (Figure 6).

[23] The seasonal variations in ozone are generally in good agreement with the variations in solar radiation (Figure 3) and satellite retrieved lower tropospheric CO and tropospheric column NO_2 (Figure 7). Like ozone, all these parameters show an increasing tendency from January to May, decrease to lower levels during June–September and increase again during October–December. These variations suggest that the coupling of higher solar radiation with higher levels of precursor gases lead to enhanced daytime photochemical ozone production and thus higher ozone levels are observed during spring and autumn. Lower levels of all the species observed during July–September are largely due to Asian monsoonal circulation, which leads to inflow of pristine marine air masses in this region and also suppresses the photochemical activity through widespread cloudy/rainy conditions. The arrival of marine air masses over this region is evident from the back-air trajectory analysis (Figure 2) and occurrence of highest rainfall at Pantnagar (Figure 3) during these months. During January, this region is generally covered by thick fog and lowest ozone levels observed during this month could be due to fog-induced suppression of photochemical activity as also indicated by ozone diurnal variation for January (Figure 4). The increase in nighttime levels during spring months suggest for an overall increase in the regional background ozone. This could be due to higher ozone production on the regional scale of northern India [*Kumar et al.*, 2010] and occurrence of significantly higher biomass burning activity during spring [*Kumar et al.*, 2011] in this region. The difference between daytime and nighttime monthly average ozone levels can be termed as photochemical buildup at this site and shows large variability with values as low as 9–14 ppbv during August–September and as high as 32–41 ppbv during spring and autumn months (Table 3 and auxiliary material Table S1).

[24] Here it can be noted that during spring and autumn seasons, when ozone levels (and precursors) show primary and secondary peaks respectively, air masses mostly circulate over the continental Indian region including polluted IGP region before reaching (within 1–2 days) at the observation site (Figure 2). Thus, the air masses, being well exposed to the regional emissions of this region, could be

Table 3. Monthly Average Ozone During Nighttime, Daytime at Pantnagar, Monthly Average Ozone at Nainital (24 h), and Photochemical Ozone Buildup at Pantnagar in Different Months

Month	Nighttime Ozone at Pantnagar (ppbv)	Daytime Ozone at Pantnagar (ppbv)	Average Ozone at Nainital (ppbv)	Photochemical Ozone Buildup at Pantnagar (ppbv)
January	4.9 ± 4.5	21.4 ± 15.5	37.9 ± 6.9	16.5
February	7.8 ± 7.5	35.6 ± 11.4	46.0 ± 8.0	27.8
March	13.4 ± 8.6	50.4 ± 12.1	54.6 ± 13.2	37.0
April	18.4 ± 9.1	57.9 ± 13.6	59.2 ± 12.6	39.5
May	25.5 ± 11.9	57.2 ± 16.6	62.2 ± 10.3	31.7
June	22.8 ± 11.4	51.8 ± 17.4	62.2 ± 13.3	29.1
July	13.5 ± 7.2	27.4 ± 15.0	28.6 ± 11.5	13.9
August	11.9 ± 6.5	21.8 ± 7.6	24.1 ± 7.9	9.9
September	14.6 ± 9.9	24.5 ± 10.0	26.6 ± 8.6	9.9
October	7.1 ± 4.4	44.4 ± 14.4	38.8 ± 7.3	37.4
November	7.3 ± 5.2	48.7 ± 13.8	38.1 ± 5.9	41.4
December	4.9 ± 4.2	42.6 ± 11.8	39.4 ± 11.6	37.7

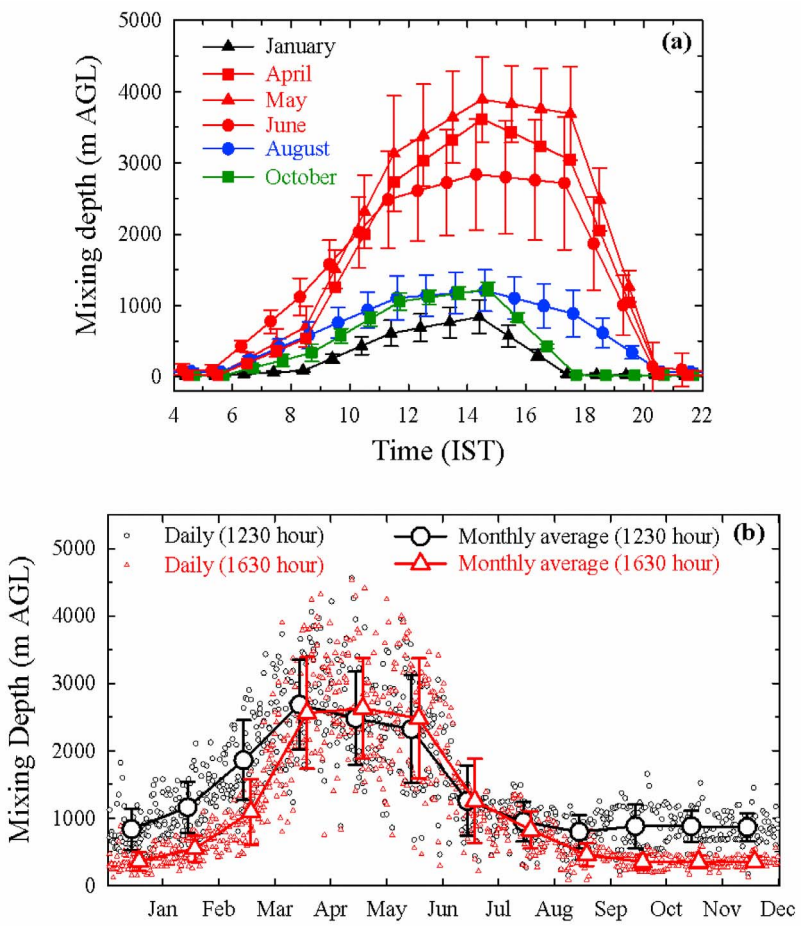

Figure 8. (a) Average diurnal variations in mixing depth at Pantnagar during four different months (January, April, August and October) representing four seasons. Two additional months (May and June) are also shown. (b) Seasonal variations in the daily and monthly average mixing depth at Pantnagar. Mixing depth is obtained from GDAS data.

rich in ozone and precursors. However, the secondary ozone peak observed during autumn is not as high as that during spring. Notably, the solar radiation is less intense during autumn as compared to spring. In addition, biomass burning activities are highest during spring over this region, when compared with the biomass burning during autumn [*Kumar et al.*, 2011].

3.2.1. Correlation Between Ozone and Mixing Depth

[25] The diurnal and seasonal variations in the mixing depth over Pantnagar are shown in Figure 8. As expected, mixing depth starts growing gradually after the sunrise, evolves rapidly during 0800–1200 h to attain maximum values during noontime and decreases thereafter. Mixing depth is as high as about 4 km during noontime of May while it is only about 0.9 km during January. Mixing depth is also lower during August and October. Mixing depth remains very low (50–100 m) during nighttime and unlike daytime, nighttime mixing depth remains nearly similar in all the months. The monthly average mixing depth is highest (about 2500 m) during April and May while it is less than 1500 m during rest of months (Figure 8b and Table 1). The highest daytime mixing depth during spring is in agreement with the seasonal variation in solar radiation and temperature at this site. The mixing depth during the 1630 h is somewhat lower than the mixing depth during the 1230 h in autumn and winter. This is mainly due to a lower temperature and hence reduced boundary layer mixing during the afternoon period in autumn and winter.

[26] Higher ozone levels during spring and autumn are mainly attributed to the photochemical ozone production, however, boundary layer mixing processes could also contribute to the observed ozone variabilities. Boundary layer mixing can lead to some enhancements in near surface ozone levels by mixing it with the ozone-rich air aloft [*Zhang and Rao*, 1999; *Rao et al.*, 2003]. In general, ozone seasonal variations are in good agreement with those in the mixing depth until the end of the monsoon period. Ozone and the mixing depth both show a systematic increase from winter to spring. A decreasing tendency in their values begins in mid June and remains low during monsoon period. Diurnal amplitude in ozone and mixing depth also follow similar trend (Figures 4 and 8a). After September, ozone level increases, particularly in daytime but the mixing depth remains almost steady. Therefore, despite a lower mixing depth during October, November and December, there is a significant increase in the ozone value suggesting minimal role of boundary layer processes in ozone enhancement during autumn.

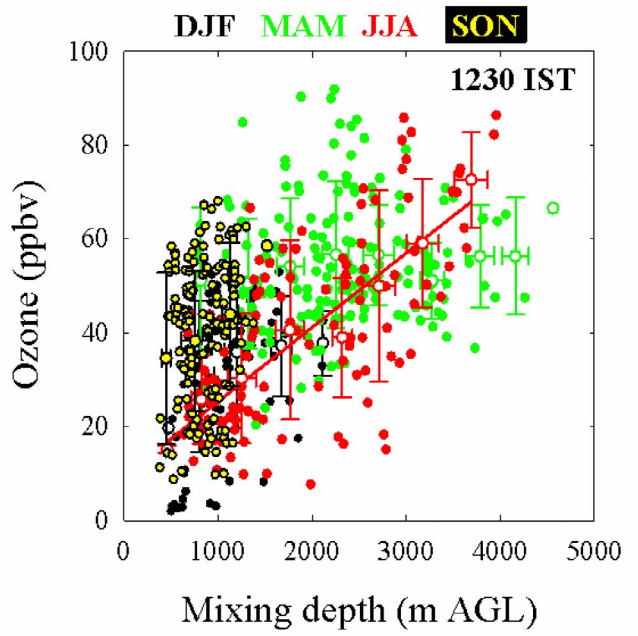

Figure 9. Correlation between daytime average ozone and the mixing depth at 1230 h IST in different seasons at Pantnagar. Filled symbols are daytime average data and open symbols are binned average data for the respective season. The r^2 has been estimated for the binned average data points. In the binned average data points, one sigma horizontally spread is in the bins of 500 m mixing depth and one sigma vertical spread is in the associated ozone data.

[27] Figure 9 shows the correlation between daytime average ozone and the mixing depth during four seasons. The ozone data has been binned corresponding to bins of 500 m mixing depth to calculate coefficient of determination (r^2). The calculation of binned average allows for smoothing the random variations in observations. The r^2 value is 0.90 for annual data and it is highest (0.96) during the summer-monsoon (June–July–August). Among June, July and August, higher ozone levels and higher mixing depths belong to June when dry weather conditions prevail around the observing site. Lower levels occur in July and August when both the boundary layer mixing and photochemical ozone production are suppressed by cloudy-rainy conditions due to arrival of southwest monsoon at the site. Depending upon the relative ozone abundances in the near surface air and the air present at higher altitudes, the variability in boundary layer height can influence the surface ozone levels. Here, average ozone levels are observed to be significantly higher at a nearby high altitude site Nainital (~2 km amsl) as compared with average surface ozone at Pantnagar (Figure 6). Thus, the deeper boundary layer can enhance the ozone levels at the surface by mixing near surface air with the ozone rich air aloft. This enhancement in surface ozone, due to daytime convective mixing, would supplement the ongoing ozone production at Pantnagar. While, a shallower boundary layer would prevent such mixing and also lead to trapping of the ozone in a smaller volume, followed by an increase in the dry deposition flux of ozone. A group of data with a large spread in ozone but very limited mixing depth range is seen in autumn and somewhat in winter too. This comparative analysis suggests that boundary layer mixing also plays a role in the observed ozone variabilities apart from that of photochemistry.

3.3. Comparison With Observations at Other Sites in India

[28] Seasonal variation in surface ozone observed at Pantnagar are compared with those at other sites namely Delhi (28.35°N, 77.12°E) [*Ghude et al.*, 2008], Gadanki (13.5°N, 79.2°E) [*Naja and Lal*, 2002], Nainital (29.37°N, 79.45°E) [*Kumar et al.*, 2010] and Trivandrum (8.55°N, 77°E) [*David and Nair*, 2011] in India (Figure 10). Delhi, Gadanki and Trivandrum are representative of urban, rural and coastal environments respectively. Nainital is a high altitude (1958 m amsl) site in the central Himalayas. Generally, sites in the Northern Indian region and having proximity to the IGP region (Pantnagar, Nainital and Delhi) show higher ozone levels during spring whereas sites in Southern India (Gadanki and Trivandrum) show higher ozone levels during winter. Additionally, seasonal amplitudes are rather higher over the sites in the Northern region, when compared with amplitudes at sites in the Southern region. Thus, the processes controlling ozone levels over the northern Indian region including IGP are different from those over the southern India.

3.3.1. Ozone at Pantnagar and Nainital

[29] The seasonal variation in monthly average ozone at Pantnagar is similar to that observed at Nainital, a high altitude site (29.37°N, 79.45°E, 1958 m amsl) in the central Himalayas, except during autumn when a secondary maximum discerned at Nainital (Figures 6 and 13 and Table 3). Further, monthly average ozone levels are significantly higher (8 to 28 ppbv) at Nainital, when compared with those at Pantnagar.

[30] Nainital is a high altitude site and relatively longer lifetime of ozone could be a major factor in displaying higher levels at Nainital. Unlike the all data average ozone, daytime average ozone at Pantnagar shows a secondary maximum during autumn that is similar to the observation at Nainital. Since, in situ photochemical ozone production is little at Nainital [*Kumar et al.*, 2010]; the similarity between the ozone data at Pantnagar and Nainital indicates a possible role

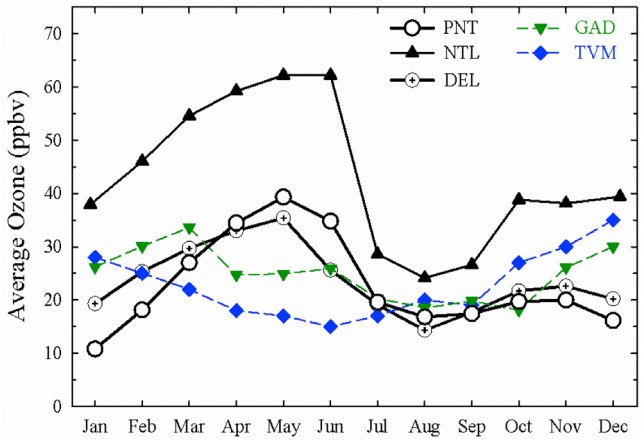

Figure 10. Comparison of the observed monthly average ozone seasonal variations at Pantnagar (PNT) with the observations at other sites Nainital (NTL), Delhi (DEL), Gadanki (GAD) and Trivandrum (TVM) in India.

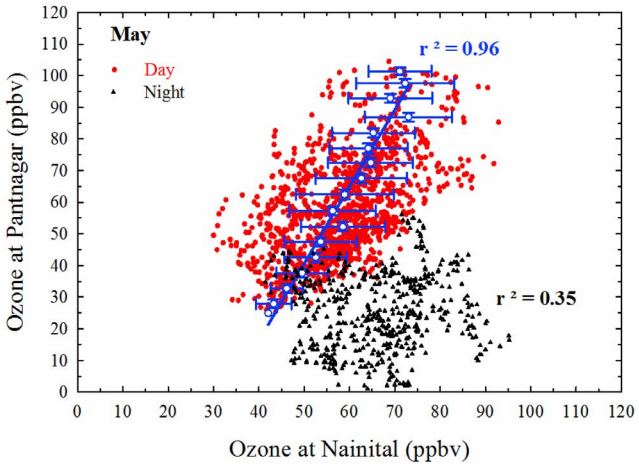

Figure 11. Correlation between ozone mixing ratios at Nainital and Pantnagar during afternoon hours (1130–1630 h) and nighttime (01–03 h) in May. Open symbols are binned average in 5 ppbv bins and error bars represent one-sigma spread in the binned data.

of convective mixing in transporting ozone and precursors from the IGP to the central Himalayas. Particularly, daytime average ozone is higher (3–10 ppbv) at Pantnagar than the average ozone at Nainital during October–December (Table 3).

[31] The boundary layer evolves fully during afternoon hours and the mixing depth at Pantnagar is even higher than the altitude of Nainital during spring (Figure 8a). The daytime mixing depth is as high as 3890 m in May. Additionally, daytime (1130–1630 h) ozone levels observed at Pantnagar and Nainital are seen to have strong positive correlation (r^2 = 0.96) during May, while no clear relationship is seen during the nighttime (Figure 11). The r^2 value is estimated using 5-ppbv binned ozone data. Horizontal and vertical error bars show 1 sigma spread in the bins of 5-ppbv. Since Nainital and Pantnagar are separated by only about 30 km, air masses over Pantnagar and Nainital could be well mixed during daytime and show a strong positive correlation. During the nighttime, the shallower boundary layer at Pantnagar decouples its atmosphere from that of Nainital and there is no clear relationship between them. The above analysis suggests that emissions and photochemical processes occurring in the IGP can influence the air quality of the Himalayan region, particularly during spring mid-day, when the convective mixing is the strongest in this region.

3.4. Results From a Global Chemistry Transport Model (MATCH-MPIC)

[32] The spatial distributions of MATCH-MPIC simulated monthly mean surface ozone over the South Asian region for January, April, July and October, representing the winter, spring, summer-monsoon and autumn seasons respectively, are shown in Figure 12. During January, ozone levels are lower (20–40 ppbv) over northern India while levels are higher (40–50 ppbv) over central India and much higher (above 60 ppbv) over the coastal Arabian Sea and the northern part of Bay of Bengal.

[33] Such higher ozone levels over the oceans (50–60 ppbv and higher) were also noticed during the INDOEX (Indian Ocean Experiment) observations [*Lal and Lawrence*, 2001] and other campaigns [*Naja et al.*, 2004; *Srivastava et al.*, 2011], and is mainly explained by en-route photochemical ozone production in the continental outflow. In absence of NO_x sources in the marine boundary layer, chemical losses of ozone are minimal in the transported plumes, in contrast with the nearby coastal cities, where ongoing NO_x emissions would lead to significant chemical losses of ozone. Occasionally, there could be some contribution from the downward transport of ozone rich air from the free troposphere in producing such high levels of surface ozone as suggested by *Lal and Lawrence* [2001] and reported observationally over Bay of Bengal by *Sahu and Lal* [2006]. Similar feature was also seen over the Mediterranean Sea versus the nearby European polluted continental regions [*Lawrence et al.*, 2003].

[34] From winter to spring, ozone levels increase over most of South Asia and elevated levels are seen over the IGP (50–60 ppbv and more) and parts of Nepal and Burma while they decrease over the oceanic regions (20–40 ppbv). During the summer/monsoon, the arrival of cleaner marine air mass results in the lowest ozone levels (20–40 ppbv) over most of the Indian region but higher ozone levels can still be seen in northern part of South Asia and China, indicating that these regions are not much influenced by the monsoonal circulation. During autumn, ozone levels again show a recovery over most of the Indian region with the recovery of solar radiation and pollution loadings, including ozone precursors. Model simulated spatial distributions in CO and NO_x are more-or-less similar to the ozone spatial distribution (auxiliary material Figures S2 and S3), except that the CO levels are higher in winter. Model simulations also show elevated levels of CO and NO_x over the IGP region; however, their highest levels are observed during winter and autumn.

[35] The variability of modeled surface ozone around Pantnagar in the model results is qualitatively similar to the observed variations at Pantnagar with lower values in winter and summer/monsoon and higher values during spring and autumn (Figure 13). This figure also shows the variations in daytime and nighttime monthly average ozone at Pantnagar along with monthly average surface ozone at Nainital. Apart from agreement in the seasonal variabilities, the model overestimates the observed values during all the months (e.g., by ~22 ppbv in May and by ~12 ppbv in August).

[36] Ozone diurnal variations from the model results are also compared with the observations during few months (auxiliary material Figure S4) to investigate the cause of higher ozone levels in the model results. The nighttime model values are found to be significantly higher (e.g., by ~20 ppbv in May) than the observed levels. Thus, it appears that higher model values during nighttime are likely leading to the overestimation of average ozone. Higher ozone levels during the nighttime could be due to the underestimation of model NO_x emissions over this region, leading to less titration of ozone by NO during nighttime. As mentioned earlier (Section 3.1.1), based on the observed ozone decrease rate, NO levels are expected to be high over the IGP region; further observations would be needed to confirm this possibility. The model result is, however, in good agreement with daytime ozone at Pantnagar and the average ozone at Nainital. This may be due to the coarse spatial resolution of

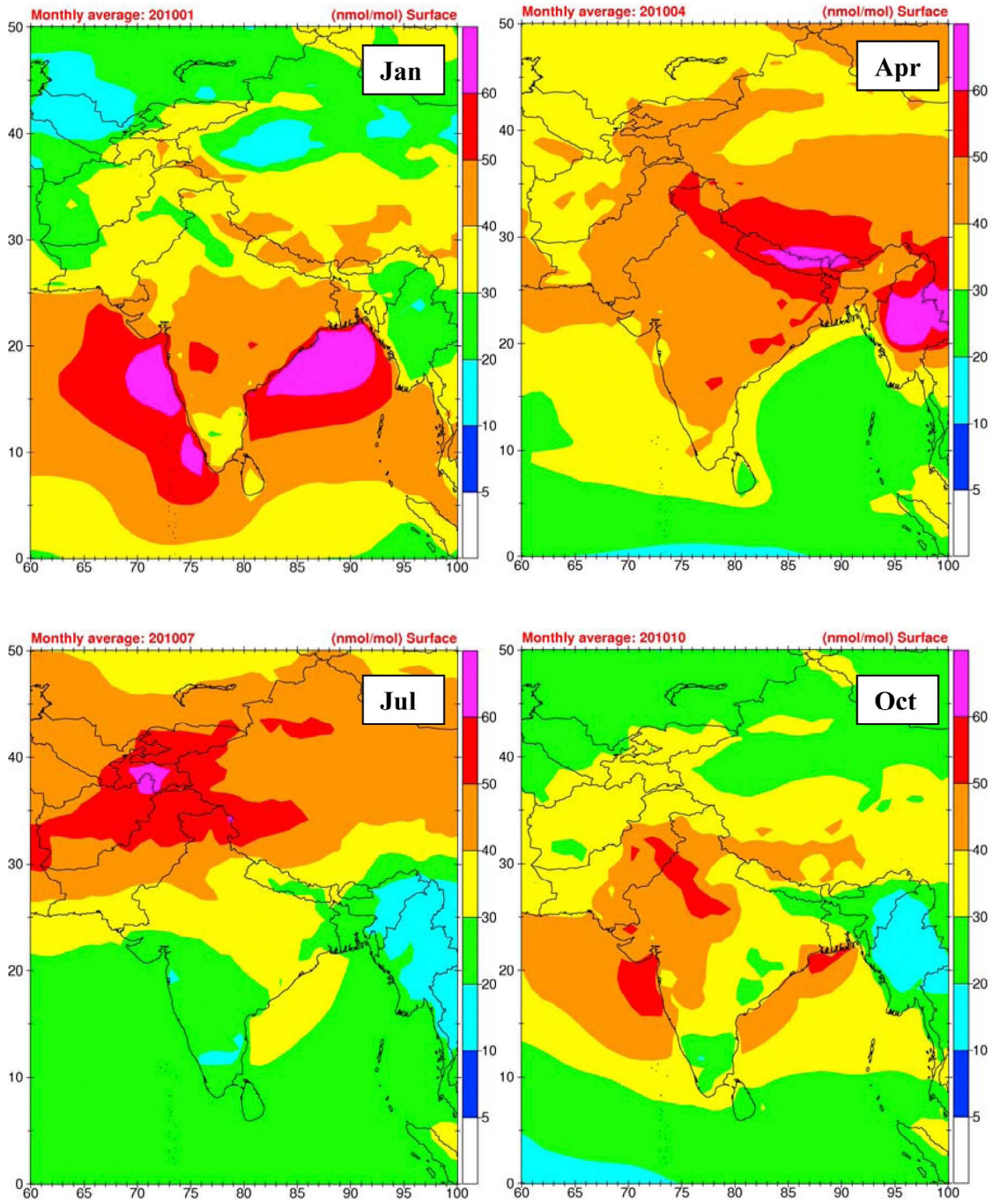

Figure 12. MATCH-MPIC simulated spatial distribution of surface ozone over the South Asian region, during four different months January, April, July and October representing four seasons, of the year 2010.

the model, which means it is not able to adequately resolve the urban environment of the IGP from the nearby cleaner mountains. Topography is very complex in this region and surface altitude increases by about 1700 m within a short span of about 10 km. Additionally, the October–November secondary maximum is more prominent in the model than in the observations at Pantnagar. Model results of tracer based analysis shows higher levels of biomass burning and fossil fuel CO during autumn over this region (auxiliary material Figure S5). Summarizing, though the model seems broadly representative of the ozone observations, there are differences between the model and observations, due to several factors, especially uncertainties in magnitude and ratios of emissions, the relatively coarse spatial resolution (despite being high resolution for a global model) which leads to errors in the treatment of the complex regional meteorology.

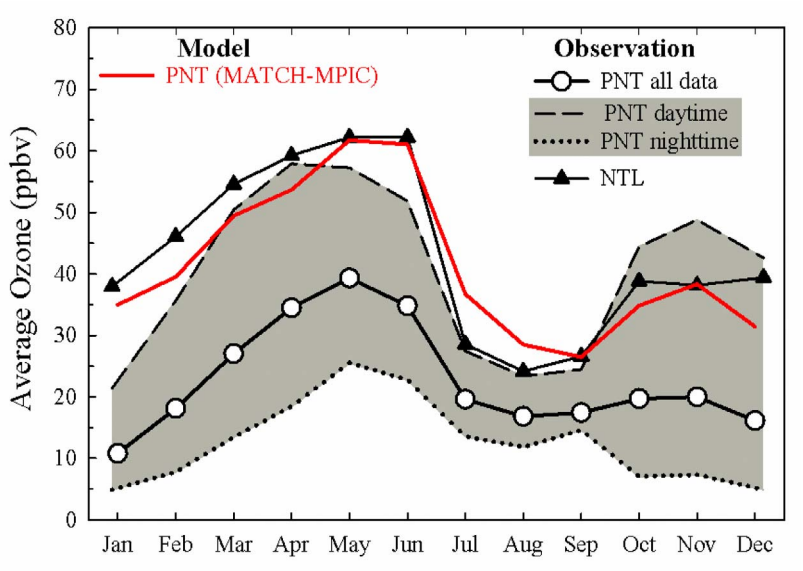

Figure 13. Comparison of the observed ozone seasonal variation at Pantnagar (PNT) with the results from MATCH-MPIC model. Seasonal variation in ozone, at a nearby high altitude site Nainital, is also shown. Upper range and lower range in gray shaded region is daytime and nighttime ozone data at Pantnagar, respectively.

3.4.1. Variations in H_2O_2 and HNO_3 From MATCH-MPIC

[37] The variations in H_2O_2 and HNO_3 can be used as indicators of the sensitivity of ozone production to NO_x and hydrocarbons [*Sillman*, 1995]. In the urban environments, major sources of odd hydrogen species, i.e., the sum of OH, HO_2 and RO_2 [*Kleinman*, 1986, *Sillman et al.*, 1990, *Sillman*, 1991] are ozone photolysis followed by reaction of $O(^1D)$ with water vapor and the photolysis of aldehydes and other intermediate reactive organic compounds. Major sink reactions for odd hydrogen are the following -

(R1) $$HO_2 + HO_2 \rightarrow H_2O_2 + O_2$$

(R2) $$RO_2 + HO_2 \rightarrow ROOH + O_2$$

(R3) $$OH + NO_2 \rightarrow HNO_3$$

[38] In addition to the reactions from (R1) to (R3), formation of PAN (Peroxyacetylnitrate) could also be a significant sink for the odd hydrogen. The nature of ozone chemistry as NO_x-sensitive or hydrocarbon-sensitive would be determined by the relative rates of formation of peroxides (R1) and (R2) and nitric acid (R3) and to their contribution as sinks for odd hydrogen. Generally, noontime values of H_2O_2 to HNO_3 ratios less than 0.4 are found to be associated with the hydrocarbon-sensitive ozone chemistry, while values higher than 0.4 are associated with the NO_x-sensitive chemistry [*Sillman*, 1995].

[39] Seasonal variations in MATCH-MPIC simulated daytime (1130–1630 h) daily and monthly average values of H_2O_2, HNO_3 and H_2O_2/HNO_3 ratio at Pantnagar for the year 2010 are shown in Figure 14. H_2O_2 shows nearly similar seasonality to that of ozone with higher values during spring (2.7 ± 0.9 ppbv in May) and autumn (2.0 ± 0.7 ppbv in October) and lower values during winter (0.5 ± 0.3 to 0.9 ± 0.4 ppbv) and summer/monsoon (1.1 ± 0.5 ppbv in August). The variations in HNO_3 values are more-or-less similar to those in ozone except in winter. HNO_3 values are higher during spring (1.4 ± 0.5 ppbv in May) and autumn (1.5 ± 0.7 ppbv in November) and lowest during summer/monsoon (0.1 ± 0.1 ppbv in August). Most of the time, daytime daily average values of H_2O_2/HNO_3 ratios are more than one except during early winter and late autumn. Generally, average H_2O_2/HNO_3 values range from 1.1 ± 0.7 to 2.9 ± 1.5, except during summer-monsoon, and are well above the critical limit of 0.4 [*Sillman*, 1995] indicating that ozone chemistry over this region is NO_x-limited. Higher ratios during summer-monsoon (16.3 ± 13.4 to 39.5 ± 108.0) are mainly due to very low values of HNO_3 associated with long range transport of cleaner marine air masses and possibility of enhanced wet depositional losses of HNO_3 in the heavy rainfall (Figures 2 and 3) during the summer-monsoon. The sensitivity of ozone chemistry to NO_x at Pantnagar will further be shown using sensitivity simulations from a chemical box model in the next section.

3.5. Photochemical Ozone Production Rate and Sensitivity to NMHCs and NO_x

[40] Ozone levels depend nonlinearly on the concentrations of its precursors including hydrocarbons, CO and NO_x [*Lin et al.*, 1988; *Chameides et al.*, 1992; *Sillman*, 1999] and thus ozone control policies in urban and rural regions are region specific and difficult to design. Here, we attempt to characterize the dependence of surface ozone on NMHCs and NO_x by combining the available observations, emissions over this region and using a chemical box model. A chemical box-model is set-up to simulate the diurnal variation of ozone at Pantnagar to lend confidence into the use of model for the aforementioned sensitivity study.

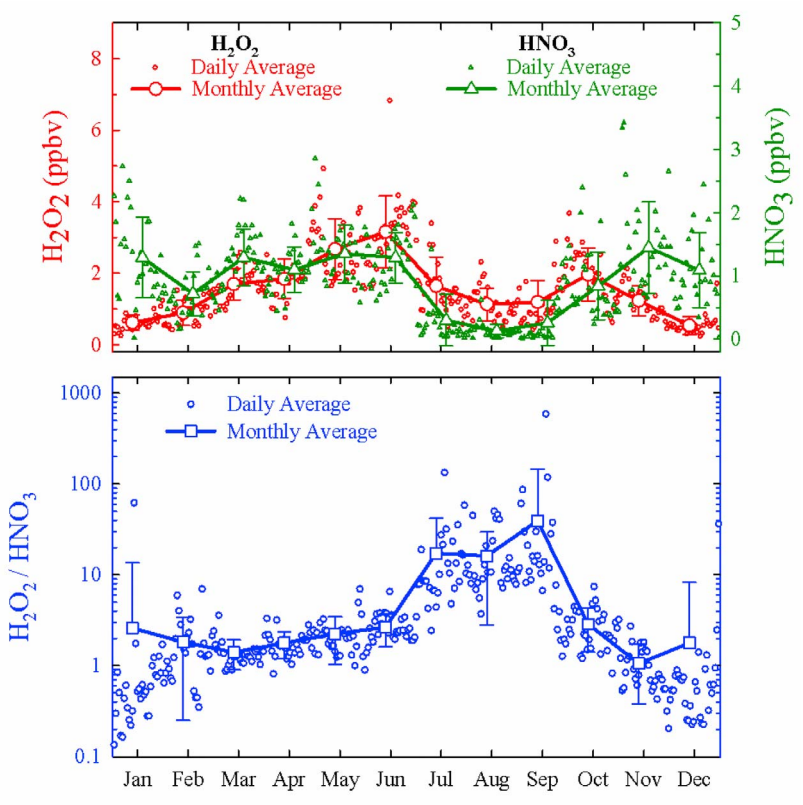

Figure 14. MATCH-MPIC simulated variations in daytime (1130–1630 h) H_2O_2, HNO_3 and H_2O_2/HNO_3 ratios at Pantnagar during January to December 2010.

[41] The environmental conditions of typical spring (April) are selected for the box model simulations at Pantnagar (Table 4). The overhead total column ozone is set to the value obtained from OMI. The model is initialized with the observed concentrations of CO, NO_x, CH_4 and few light non-methane hydrocarbons (C_2–C_5) at this site while other species are assumed and set to the typical values of a semi-urban environment. Anthropogenic emissions of CO, NO_x and hydrocarbons from Intercontinental Chemical Transport Experiment–Phase B (INTEX-B) emission inventory [*Zhang et al.*, 2009] are used. Since INTEX-B emissions are representative of the year 2006 and analysis of historic emissions (1980–2003) from Regional Emission Inventory for Asia (REAS) [*Ohara et al.*, 2007] indicates an increase of about 8% per year in NO_x emissions over India, therefore NO_x emissions are increased by 40% for this study. Figure 15 shows chemical box model simulated diurnal ozone variation. The modeled (base run) diurnal variation is in good agreement with the observations. However, model values are lower during mid-night. This model run is shown as "base run" in Figure 15. The instantaneous production (P), loss (L) and net production (P-L) rates of ozone [*Duderstadt et al.*, 1998; *Kanaya et al.*, 2009] are also calculated for this base run as follows and shown in Figure 16.

$$P\,(O_3) = k_1[HO_2]\,[NO] + \sum k_{2i}[RO_2]_i[NO] \quad (1)$$

$$L\,(O_3) = k_3\left[O^1(D)\right]\,[H_2O] + k_4[OH]\,[O_3] + k_5[HO_2]\,[O_3] \quad (2)$$

$$P - L\,(O_3) = P\,(O_3) - L\,(O_3) \quad (3)$$

where k_1 to k_5 are the rate coefficients of the HO_2 + NO, RO_2 + NO, $O^1(D)$ + H_2O, OH + O_3 and HO_2 + O_3 reactions, respectively.

[42] The ozone production rate $P(O_3)$ starts increasing rapidly after sunrise to about 1000 h and thereafter it decreases. Highest values of $P(O_3)$ are observed to be 14.5 ppbv h^{-1} during 0900–1000 h. Total ozone produced during daytime (0800–1600 h) is estimated by converting these instantaneous $P(O_3)$ values to hourly averages and then integrating from 0800 to 1600 h. This way, the total ozone produced in the daytime is 81.2 ppbv. The ozone loss rate $L(O_3)$ shows an increasing tendency slightly later than $P(O_3)$ and shows a symmetric decreasing trend unlike $P(O_3)$. The total ozone loss per day is 8.3 ppbv. The rate of net ozone production i.e.,

Table 4. Environmental Conditions, Representing Spring, Opted for the Chemical Box Model Simulations

Characteristic	Value
Temperature	298 K
Relative Humidity	50%
Surface albedo	0.10
Parcel elevation	500 m
Overhead O_3 column	262 DU (OMI)
Aerosol optical depth at 550 nm (vertical, total)	0.235 (for continental aerosol)
Aerosol Angstrom coefficient	1
Aerosol single scattering albedo	0.99

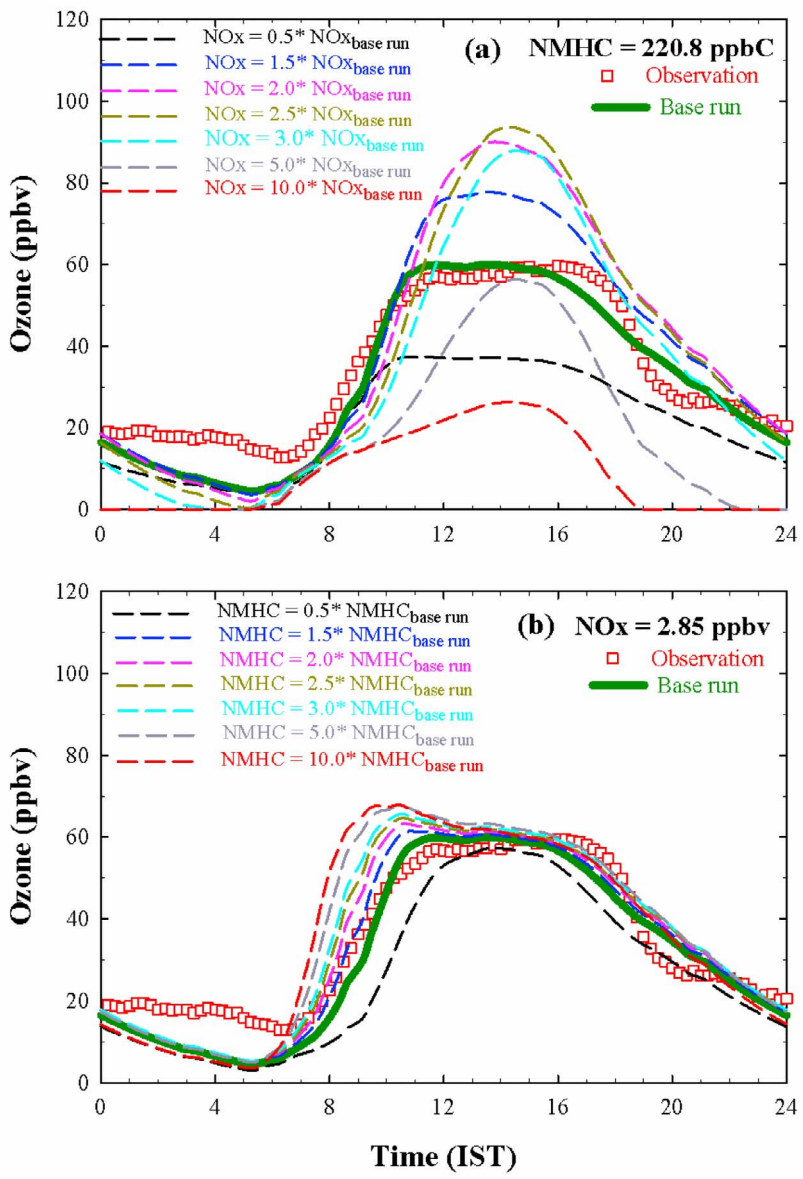

Figure 15. Box model simulated diurnal variations in surface ozone. Apart from the base run, diurnal variations in ozone for (a) different levels of NO_x and constant level of NMHCs and (b) different levels of NMHCs and constant level of NO_x are also shown.

P-L(O_3) follows similar variations as that in the P(O_3) with highest values of P-L(O_3) of 13.9 ppbv h^{-1} during 0900–1000 h. Integrated net ozone production in a day is 72.9 ppbv. Accumulated ozone calculated from the observed rate of change of ozone (Figure 5b) during 0800–1600 h is 45.4 ppbv. The difference in these two quantities, integrated ozone from box model and observations, (~27.5 ppbv) can be attributed to the physical and dynamical processes, which are not considered in the chemical box model simulations.

[43] Apart from the base run, two sets of sensitivity simulations are also conducted. One set of runs is made by keeping NMHCs constant at the values of the base run (220.8 ppbC) with varied NO_x levels between 0.5 to 10 times of the base run NO_x value (2.85 ppbv). A second set of runs was made by keeping NO_x value constant at its base run value (2.85 ppbv) with varied NMHCs levels between 0.5 to 10 times of the base run value of NMHCs. These two sets of simulations along with the base run are shown in Figure 15.

[44] Model simulated ozone diurnal variations for varying NO_x levels shows rapid increase in the daytime ozone levels from ~37 ppbv (for 0.5*$NO_{x\ base\ run}$ case) to ~93.5 ppbv (2.5*$NO_{x\ base\ run}$) (Figure 15a). In contrast, when NO_x levels are increased further, ozone levels start decreasing from ~88 ppbv (for 3*$NO_{x\ base\ run}$) to ~26 ppbv (10*$NO_{x\ base\ run}$). Apart from changes in ozone levels, daytime variations also change from a broad pattern to a peak type of pattern, when increasing NO_x levels. In contrast to the sensitivity tests for varying NO_x levels, ozone diurnal variations and its levels do not show significant changes for varying the levels of NMHCs (Figure 15b). Ozone levels show only a small

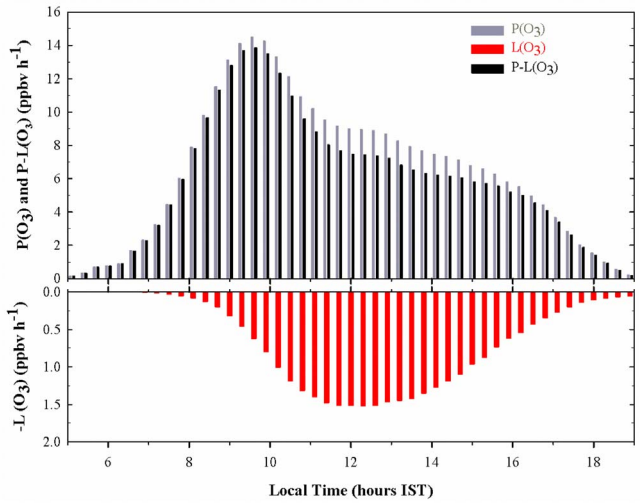

Figure 16. Diurnal variations in ozone production rate $P(O_3)$, ozone loss rate $L(O_3)$ and net ozone production rate $P\text{-}L(O_3)$ estimated from box model simulations for the base run.

increase (~5 ppbv) from ~57 ppbv (for 0.5*NMHC $_{\text{base run}}$) to ~62.5 ppbv (for 10*NMHC $_{\text{base run}}$) for whole range of NMHCs. The above analysis indicates that ozone production chemistry is NO_x limited in this region, while variations in the levels of hydrocarbons play a minor role in affecting ozone levels.

4. Discussions and Conclusions

[45] Observations of surface ozone were made at a semi-urban site (Pantnagar) in the Indo-Gangetic plain region during March 2009–June 2011 and these data were analyzed using meteorological parameters, backward trajectories, space-borne observations, results from a global chemistry transport model and a photochemical box model. Ozone diurnal variations were characterized by daytime photochemical build up. The rate of change of ozone during morning (+5.6 ppbv hr^{-1}) and evening time (−8.5 ppbv hr^{-1}) are dissimilar and a higher ozone loss rate in the evening suggests that ozone loss processes could be stronger over the IGP due to high NO_x emissions.

[46] The seasonal variations in daily and monthly average ozone at Pantnagar show a systematic increase from January to May, decrease sharply to lower levels during June–September then a slight increase during October–November. Notably, daytime ozone shows prominent secondary maxima during October–November which is not seen in the all data. Ozone levels are observed to be highest during the spring months (39.3 ± 18.9 ppbv in May) and lower during the summer/monsoon (16.8 ± 8.9 in August) and winter (10.8 ± 12.1 ppbv in January). Monthly average values are mostly below 40 ppbv; however, occasionally hourly average ozone levels are in the range of 80–100 ppbv, particularly during spring. CO levels are observed to be moderately high (188–484 ppbv) while CH_4 values range from 1.81 to 2.11 ppmv.

[47] Observed ozone seasonality is in good agreement with the solar radiation and satellite derived lower tropospheric CO and tropospheric column NO_2. Lower levels of all the gases during July–September are mainly attributed to the arrival of southwest monsoon bringing cleaner marine air to this region. During spring and autumn, air masses mostly circulate over the continental Indian region, including the IGP, before reaching to the observation site and thus could be rich in ozone and precursors. However, the spring peak is higher than the autumn peak that could be due to the presence of additional ozone precursors from biomass burning and intense solar radiation during spring when compared with those during autumn [*Kumar et al.*, 2011]. In addition to photochemistry, boundary layer dynamics could also play a role in the observed ozone variabilities. The lower mixing depth during autumn suggests a minimal role of the boundary layer processes in ozone enhancement during autumn. A correlation analysis shows a positive relationship between ozone mixing ratios and mixing depth, suggesting that some enhancement in the near surface ozone could be due to its mixing with the ozone rich air aloft in a deeper boundary layer.

[48] A comparison of ozone observations at Pantnagar, with a nearby high altitude site Nainital, located in the central Himalayas, was also made. It was found that the daytime (1130–1630 h) ozone at Pantnagar shows variability and levels similar to those at Nainital. Ozone mixing ratios at Pantnagar and Nainital show strong positive correlation in the daytime, during spring when mixing depth over Pantnagar is also higher, while nighttime ozone mixing ratios do not show a clear relationship. This indicates that emissions and photochemical processes in the IGP region can influence the air quality over the cleaner Himalayan region via boundary layer mixing processes. Comparison of the ozone seasonal variation at Pantnagar with other sites in India shows that sites in the Northern Indian region, having proximity to the IGP region, have maximum ozone levels during spring, while sites located in the southern part of India show maximum ozone levels during winter. This comparison highlights the diversity of emissions as well as processes controlling ozone levels over different parts of Indian region.

[49] A global chemistry transport model (MATCH-MPIC) has been used to simulate the spatial and temporal variabilities in ozone and related species over this region. The model reproduces the overall springtime elevated ozone levels over the IGP, lower ozone during the summer/monsoon and winter, and a recovery phase during autumn. However, the model overestimates the ozone levels during all the months, which is attributed to the higher ozone levels in the model during nighttime. This could be due to a possible underestimation of NO_x emissions resulting in less ozone titration. In addition, model ozone shows a more pronounced secondary maximum during autumn. CO-tracer based analysis suggests that this overestimation in the model could be associated with the biomass burning. The MATCH-MPIC output is further used to assess the variabilities in H_2O_2 and HNO_3 as an indicator of ozone sensitivity to hydrocarbons and NO_x. Average values of H_2O_2/HNO_3 ratios range from 1.1 ± 0.7 to 2.9 ± 1.5, which suggests that ozone chemistry over this region is NO_x-limited.

[50] Further, simulations from a chemical box model are used to estimate ozone production and loss rates at Pantnagar and to study the ozone sensitivity with changes in NO_x and

NMHCs. Integrated net ozone production, from model, in a day, is estimated to be 72.9 ppbv while it is about 45.4 ppbv from the observation. The difference in these two quantities (~27.5 ppbv) is suggested to be due to other physical and dynamical processes, which are not considered in the chemical box model. A set of sensitivity simulations further confirms that this site is in the NO_x-limited regime and variations in the levels of hydrocarbons play a minor role in affecting ozone levels.

[51] The present study is the first attempt to understand the ozone photochemical production in the Indo-Gangetic Plain (IGP) using measurements and model simulations. More detailed, continuous and systematic measurements of ozone and its precursors are desirable over this region to improve our understanding of the chemical and dynamical processes, spatiotemporal variabilities and their implications for regional and global climate. An impact assessment of the pollution load and its effects on the crop yields is essential over this IGP region, which is also a region dominated by agricultural activities. Global model studies have shown that losses in global crop production could be 79–121 million metric tons per year, i.e., amounting to about 11–18 billion USD during 2000 [*Avnery et al.*, 2011]. Therefore, it is highly essential to plan ozone control strategies even on regional scales.

[52] **Acknowledgments.** We are highly thankful to Sasha Madronich and coworkers for development of the NCAR Master Mechanism box model. We gratefully acknowledge NOAA Air Resources Laboratory for provision of HYSPLIT model used in this study. OMI, TES and TRMM data are obtained using Giovanni. We are grateful to Ram Sagar, C. B. S. Dutt and P. P. N. Rao for encouraging this work. We thank S. Venkataramani, Ashish Kumar, Kalpana Pandey, Manav Kumar and Manjul Mungali for help in measurements. This study is carried out under ISRO-GBP ATCTM project. We thank three anonymous reviewers for their constructive comments and suggestions.

References

Adler, R. F., et al. (2000), Tropical rainfall distributions determined using TRMM combined with other satellite and rain gauge information, *J. Appl. Meteorol.*, *39*, 2007–2023, doi:10.1175/1520-0450(2001)040<2007:TRDDUT>2.0.CO;2.

Akimoto, H. (2003), Global air quality and pollution, *Science*, *302*, 1716–1719, doi:10.1126/science.1092666.

Asnani, G. C. (2005), Climatology of the tropics, in *Tropical Meteorology*, vol. 1, pp. 100–204, G. C. Asnani, Pune, India.

Avnery, S., D. L. Mauzerall, J. Liu, and L. W. Horowitz (2011), Global crop yield reductions due to surface ozone exposure: 1. Year 2000 crop production losses and economic damage, *Atmos. Environ.*, *45*, 2284–2296, doi:10.1016/j.atmosenv.2010.11.045.

Beer, R., T. A. Glavich, and D. M. Rider (2001), Tropospheric Emission Spectrometer for the Earth Observing System's Aura satellite, *Appl. Opt.*, *40*, 2356–2367, doi:10.1364/AO.40.002356.

Beig, G., S. Gunthe, and D. B. Jadhav (2007), Simultaneous measurements of ozone and its precursors on a diurnal scale at a semi urban site in India, *J. Atmos. Chem.*, *57*, 239–253, doi:10.1007/s10874-007-9068-8.

Bucsela, E. J., E. A. Celarier, M. O. Wenig, J. F. Gleason, J. P. Veefkind, K. F. Boersma, and E. J. Brinksma (2006), Algorithm for NO_2 vertical column retrieval from the Ozone Monitoring Instrument, *IEEE Trans. Geosci. Remote Sens.*, *44*, 1245–1258, doi:10.1109/TGRS.2005.863715.

Cantrell, C. A., and J. J. Orlando (1999), Hydrogen compounds, in *Atmospheric Chemistry and Global Change*, edited by G. P. Brasseur, J. J. Orlando, and G. S. Tyndall, pp. 209–234, Oxford Univ. Press, New York.

Chameides, W., et al. (1992), Ozone precursor relationships in the ambient atmosphere, *J. Geophys. Res.*, *97*, 6037–6056, doi:10.1029/91JD03014.

Crutzen, P. J., and M. G. Lawrence (2000), The impact of precipitation scavenging on the transport of trace gases: A 3-dimensional model sensitivity study, *J. Atmos. Chem.*, *37*, 81–112, doi:10.1023/A:1006322926426.

David, L. M., and P. R. Nair (2011), Diurnal and seasonal variability of surface ozone and NO_x at a tropical coastal site: Association with mesoscale and synoptic meteorological conditions, *J. Geophys. Res.*, *116*, D10303, doi:10.1029/2010JD015076.

Dentener, F. J., and P. J. Crutzen (1993), Reaction of N_2O_5 on tropospheric aerosols: Impact on the global distributions of NO_x, O_3, and OH, *J. Geophys. Res.*, *98*, 7149–7163, doi:10.1029/92JD02979.

Desqueyroux, H., J. C. Pujet, M. Prosper, F. Squinazi, and I. Momas (2002), Short-term effects of low-level air pollution on respiratory health of adults suffering from moderate to severe asthma, *Environ. Res.*, *89*, 29–37, doi:10.1006/enrs.2002.4357.

Di Girolamo, L., et al. (2004), Analysis of Multi-angle Imaging SpectroRadiometer (MISR) aerosol optical depths over greater India during winter 2001–2004, *Geophys. Res. Lett.*, *31*, L23115, doi:10.1029/2004GL021273.

Draxler, R., B. Stunder, G. Rolph, A. Stein, and A. Taylor (2012), HYSPLIT4 user's guide, version 4, report, NOAA, Silver Spring, Md. [Available at www.arl.noaa.gov/documents/reports/hysplit_user_guide.pdf.]

Duderstadt, K. A., et al. (1998), Photochemical production and loss rates of ozone at Sable Island, Nova Scotia during the North Atlantic Regional Experiment (NARE) 1993 summer intensive, *J. Geophys. Res.*, *103*, 13,531–13,555, doi:10.1029/98JD00397.

Fishman, J., A. E. Wozniak, and J. K. Creilson (2003), Global distribution of tropospheric ozone from satellite measurements using the empirically corrected tropospheric ozone residual technique: Identification of the regional aspects of air pollution, *Atmos. Chem. Phys.*, *3*, 893–907, doi:10.5194/acp-3-893-2003.

Forster, P. et al. (2007), Changes in atmospheric constituents and in radiative forcing, in *Climate Change 2007: The Physical Science Basis. Contribution of Working Group I to the Fourth Assessment Report of the Intergovernmental Panel on Climate Change*, edited by S. Solomon et al., pp. 131–234, Cambridge Univ. Press, Cambridge, U. K.

Ganzeveld, L., and J. Lelieveld (1995), Dry deposition parameterization in a chemistry general circulation model and its influence on the distribution of reactive trace gases, *J. Geophys. Res.*, *100*, 20,999–21,012, doi:10.1029/95JD02266.

Gautam, R., Z. Liu, R. P. Singh, and N. C. Hsu (2009), Two contrasting dust-dominant periods over India observed from MODIS and CALIPSO data, *Geophys. Res. Lett.*, *36*, L06813, doi:10.1029/2008GL036967.

Ghude, S. D., et al. (2008), Ozone in ambient air at a tropical megacity, Delhi: Characteristics, trends and cumulative ozone exposure indices, *J. Atmos. Chem.*, *60*, 237–252, doi:10.1007/s10874-009-9119-4.

Giles, D. M., et al. (2011), Aerosol properties over the Indo-Gangetic Plain: A mesoscale perspective from the TIGERZ experiment, *J. Geophys. Res.*, *116*, D18203, doi:10.1029/2011JD015809.

Hack, J. J., B. A. Boville, J. T. Kiehl, P. J. Rasch, and D. L. Williamson (1994), Climate statistics from the National Center for Atmospheric Research community climate model CCM2, *J. Geophys. Res.*, *99*, 20,785–20,813, doi:10.1029/94JD01570.

Holtslag, A. A. M., and B. A. Boville (1993), Local versus nonlocal boundary-layer diffusion in a global climate model, *J. Clim.*, *6*, 1825–1842, doi:10.1175/1520-0442(1993)006<1825:LVNBLD>2.0.CO;2.

Jethva, H., S. K. Satheesh, and J. Srinivasan (2005), Seasonal variability of aerosols over the Indo-Gangetic basin, *J. Geophys. Res.*, *110*, D21204, doi:10.1029/2005JD005938.

Kanaya, Y., et al. (2009), Rates and regimes of photochemical ozone production over central East China in June 2006: A box model analysis using comprehensive measurements of ozone precursors, *Atmos. Chem. Phys.*, *9*, 7711–7723, doi:10.5194/acp-9-7711-2009.

Kar, J., et al. (2010), Wintertime pollution over the Eastern Indo-Gangetic Plains as observed from MOPITT, CALIPSO and tropospheric ozone residual data, *Atmos. Chem. Phys.*, *10*, 12,273–12,283, doi:10.5194/acp-10-12273-2010.

Kleinman, L. I. (1986), Photochemical formation of peroxides in the boundary layer, *J. Geophys. Res.*, *91*, 10,889–10,904, doi:10.1029/JD091iD10p10889.

Kleinman, L., et al. (1994), Ozone formation at a rural site in the southern United States, *J. Geophys. Res.*, *99*, 3469–3482, doi:10.1029/93JD02991.

Kumar, R., M. Naja, S. Venkataramani, and O. Wild (2010), Variations in surface ozone at Nainital, a high altitude site in the Central Himalayas, *J. Geophys. Res.*, *115*, D16302, doi:10.1029/2009JD013715.

Kumar, R., M. Naja, S. K. Satheesh, N. Ojha, H. Joshi, T. Sarangi, P. Pant, U. C. Dumka, P. Hegde, and S. Venkataramani (2011), Influences of the springtime northern Indian biomass burning over the central Himalayas, *J. Geophys. Res.*, *116*, D19302, doi:10.1029/2010JD015509.

Kunhikrishnan, T., M. G. Lawrence, R. von Kuhlmann, A. Richter, A. Ladstätter-Weißenmayer, and J. P. Burrows (2004), Analysis of tropospheric NO_x over Asia using the model of atmospheric transport and chemistry (MATCH-MPIC) and GOME-satellite observations, *Atmos. Environ.*, *38*, 581–596, doi:10.1016/j.atmosenv.2003.09.074.

Lal, S., and M. G. Lawrence (2001), Elevated mixing ratios of surface ozone over the Arabian Sea, *Geophys. Res. Lett.*, *28*(8), 1487–1490, doi:10.1029/2000GL011828.

Lal, S., M. Naja, and B. H. Subbaraya (2000), Seasonal variations in surface ozone and its precursors over an urban site in India, *Atmos. Environ.*, *34*, 2713–2724, doi:10.1016/S1352-2310(99)00510-5.

Lal, S., L. K. Sahu, and S. Venkataramani (2007), Impact of transport from the surrounding continental regions on the distributions of ozone and related trace gases over the Bay of Bengal during February 2003, *J. Geophys. Res.*, *112*, D14302, doi:10.1029/2006JD008023.

Landgraf, J., and P. J. Crutzen (1998), An efficient method for online calculations of photolysis and heating rates, *J. Atmos. Sci.*, *55*, 863–878, doi:10.1175/1520-0469(1998)055<0863:AEMFOC>2.0.CO;2.

Lawrence, M. G., and P. J. Crutzen (1998), The impact of cloud particle gravitational settling on soluble trace gas distributions, *Tellus, Ser. B*, *50*, 263–289.

Lawrence, M. G., and J. Lelieveld (2010), Atmospheric pollutant outflow from southern Asia: A review, *Atmos. Chem. Phys.*, *10*, 11,017–11,096, doi:10.5194/acp-10-11017-2010.

Lawrence, M. G., P. J. Crutzen, P. J. Rasch, B. E. Eaton, and N. M. Mahowald (1999), A model for studies of tropospheric photochemistry: Description, global distributions, and evaluation, *J. Geophys. Res.*, *104*, 26,245–26,277, doi:10.1029/1999JD900425.

Lawrence, M. G., et al. (2003), Global chemical weather forecasts for field campaign planning: Predictions and observations of large-scale features during MINOs, CONTRACE and, INDOEX, *Atmos. Chem. Phys.*, *3*, 267–289, doi:10.5194/acp-3-267-2003.

Lelieveld, J., et al. (2001), The Indian Ocean Experiment: Widespread air pollution from South and Southeast Asia, *Science*, *291*, 1031–1036, doi:10.1126/science.1057103.

Lin, X., M. Trainer, and S. C. Liu (1988), On the nonlinearity of tropospheric ozone production, *J. Geophys. Res.*, *93*(D12), 15,879–15,888, doi:10.1029/JD093iD12p15879.

Madronich, S. (2006), Chemical evolution of gaseous air pollutants downwind of tropical megacities: Mexico City case study, *Atmos. Environ.*, *40*, 6012–6018, doi:10.1016/j.atmosenv.2005.08.047.

Madronich, S., and S. Flocke (1999), The role of solar radiation in atmospheric chemistry, in *Handbook of Environmental Chemistry*, edited by P. Boule, pp. 1–26, Springer, Heidelberg, Germany.

Mauzerall, D. L., and X. P. Wang (2001), Protecting agricultural crops from the effects of tropospheric ozone exposure: Reconciling science and standard setting in the United States, Europe, and Asia, *Annu. Rev. Energy Environ.*, *26*, 237–268, doi:10.1146/annurev.energy.26.1.237.

Naja, M., and S. Lal (2002), Surface ozone and precursor gases at Gadanki (13.5°N, 79.2°E), tropical rural site in India, *J. Geophys. Res.*, *107*(D14), 4197, doi:10.1029/2001JD000357.

Naja, M., D. Chand, L. Sahu, and S. Lal (2004), Trace gases over marine regions around India, *Indian J. Mar. Sci.*, *33*(1), 95–106.

Ohara, T., H. Akimoto, J. Kurokawa, N. Horri, K. Yamaji, X. Yan, and T. Hayasaka (2007), An Asian emission inventory of anthropogenic emission sources for the period 1980–2020, *Atmos. Chem. Phys.*, *7*, 4419–4444, doi:10.5194/acp-7-4419-2007.

Olivier, J. G. J., J. P. J. Bloos, J. J. M. Berdowski, A. J. H. Visschedijk, and A. F. Bouwman (1999), A 1990 global emission inventory of anthropogenic sources of carbon monoxide on 1° × 1° developed in the framework of EDGAR/GEIA, *Chemos. Global Change Sci.*, *1*, 1–17, doi:10.1016/S1465-9972(99)00019-7.

Park, M., W. J. Randel, A. Gettelman, S. T. Massie, and J. H. Jiang (2007), Transport above the Asian summer monsoon anticyclone inferred from Aura Microwave Limb Sounder tracers, *J. Geophys. Res.*, *112*, D16309, doi:10.1029/2006JD008294.

Pöschl, U., R. von Kuhlmann, N. Poisson, and P. J. Crutzen (2000), Development and intercomparison of condensed isoprene oxidation mechanisms for global atmospheric modeling, *J. Atmos. Chem.*, *37*, 29–52, doi:10.1023/A:1006391009798.

Rao, S. T., J. Y. Ku, S. Berman, K. Zhang, and H. Mao (2003), Summertime characteristics of the atmospheric boundary layer and relationships to ozone levels over the eastern United States, *Pure Appl. Geophys.*, *160*, 21–55, doi:10.1007/s00024-003-8764-9.

Rasch, P. J., and J. E. Kristjánsson (1998), A comparison of the CCM3 model climate using diagnosed and predicted condensate parameterizations, *J. Clim.*, *11*, 1587–1614, doi:10.1175/1520-0442(1998)011<1587:ACOTCM>2.0.CO;2.

Rasch, P. J., and M. G. Lawrence (1998), Recent developments in transport methods at NCAR, *Tech. Rep. 265*, Max-Planck-Inst. für Meteorol., Hamburg, Germany.

Rasch, P. J., N. M. Mahowald, and B. E. Eaton (1997), Representations of transport, convection and the hydrologic cycle in chemical transport models: Implications for the modeling of short-lived and soluble species, *J. Geophys. Res.*, *102*, 28,127–28,138.

Reddy, R. R., et al. (2008), Measurements of surface ozone at semi-arid site Anantapur (14.62°N, 77.65°E, 331 m asl) in India, *J. Atmos. Chem.*, *59*, 47–59, doi:10.1007/s10874-008-9094-1.

Rinsland, C. P., et al. (2006), Measurements of carbon monoxide (CO) distributions by the Tropospheric Emission Spectrometer Instrument onboard the Aura spacecraft: Overview of analysis approach and examples of initial results, *Geophys. Res. Lett.*, *33*, L22806, doi:10.1029/2006GL027000.

Sahu, L. K., and S. Lal (2006), Changes in surface ozone levels due to convective downdrafts over the Bay of Bengal, *Geophys. Res. Lett.*, *33*, L10807, doi:10.1029/2006GL025994.

Schmitt, A., and B. Brunner (1997), Emissions from aviation and their development over time, in *Pollutants From Air Traffic–Results of Atmospheric Research 1992–1997, Final Report on the BMBF Verbund Programm "Schadstoffe in der Luftfahrt," DLR-Mitt. 97–04*, pp. 1–301, DLR, Oberpfaffenhofen, Germany.

Schwarzkopf, M. D., and V. Ramaswamy (1993), Radiative forcing due to ozone in the 1980s: Dependence on altitude of ozone change, *Geophys. Res. Lett.*, *20*(3), 205–208, doi:10.1029/93GL00209.

Sillman, S. (1991), A numerical solution to the equations of tropospheric chemistry based on analysis of sources and sinks of odd hydrogen, *J. Geophys. Res.*, *96*, 20,735–20,744, doi:10.1029/91JD01967.

Sillman, S. (1995), The use of NO_y, H_2O_2 and HNO_3 as indicators for O_3-NO_x-VOC sensitivity in urban locations, *J. Geophys. Res.*, *100*, 14,175–14,188, doi:10.1029/94JD02953.

Sillman, S. (1999), The relation between ozone, NO_x and hydrocarbons in urban and polluted rural environments, *Atmos. Environ.*, *33*, 1821–1845, doi:10.1016/S1352-2310(98)00345-8.

Sillman, S., J. A. Logan, and S. C. Wofsy (1990), The sensitivity of ozone to nitrogen oxides and hydrocarbons in regional ozone episodes, *J. Geophys. Res.*, *95*, 1837–1851, doi:10.1029/JD095iD02p01837.

Slingo, J. M. (1987), The development and verification of a cloud prediction scheme for the ECMWF model, *Q. J. R. Meteorol. Soc.*, *113*, 899–927, doi:10.1256/smsqj.47708.

Srivastava, S., S. Lal, S. Venkataramani, S. Gupta, and Y. B. Acharya (2011), Vertical distribution of ozone in the lower troposphere over the Bay of Bengal and the Arabian sea during ICARB-2006: Effects of continental outflow, *J. Geophys. Res.*, *116*, D13301, doi:10.1029/2010JD015298.

Stamnes, K., S. Tsay, W. J. Wiscombe, and K. Jayaweera (1998), Numerically stable algorithm for discrete-ordinate-method radiative transfer in multiple scattering and emitting layered media, *Appl. Opt.*, *27*, 2501–2509.

Thompson, A. M. (1992), The oxidizing capacity of the Earth's atmosphere: Probable past and future changes, *Science*, *256*, 1157–1165, doi:10.1126/science.256.5060.1157.

van der Werf, G. R., J. T. Randerson, L. Giglio, G. J. Collatz, P. S. Kasibhatla, and A. F. Arellano Jr. (2006), Interannual variability in global biomass burning emissions from 1997 to 2004, *Atmos. Chem. Phys.*, *6*, 3423–3441, doi:10.5194/acp-6-3423-2006.

von Kuhlmann, R. (2001), Tropospheric photochemistry of O_3, its precursors and the hydroxyl radical: A 3D modeling study considering Non-Methane hydrocarbons, PhD thesis, Univ. of Mainz, Mainz, Germany.

von Kuhlmann, R., M. G. Lawrence, P. J. Crutzen, and P. J. Rasch (2003), A model for studies of tropospheric ozone and non-methane hydrocarbons: model description and ozone results, *J. Geophys. Res.*, *108*(D9), 4294, doi:10.1029/2002JD002893.

Yienger, J. J., and H. Levy (1995), Empirical model of global soil-biogenic NO_x emissions, *J. Geophys. Res.*, *100*, 11,447–11,464.

Zhang, G. J., and N. A. McFarlane (1995), Sensitivity of climate simulations to the parameterization of cumulus convection in the Canadian Climate Centre general circulation model, *Atmos. Ocean*, *33*, 407–446, doi:10.1080/07055900.1995.9649539.

Zhang, J., and S. T. Rao (1999), The role of vertical mixing in the temporal evolution of ground-level ozone concentrations, *J. Appl. Meteorol.*, *38*, 1674–1691, doi:10.1175/1520-0450(1999)038<1674:TROVMI>2.0.CO;2.

Zhang, Q., et al. (2009), Asian emissions in 2006 for the NASA INTEX-B mission, *Atmos. Chem. Phys.*, *9*, 5131–5153, doi:10.5194/acp-9-5131-2009.